NOAA Technical Memorandum NWS TDL-56

SOME PHYSICAL AND NUMERICAL ASPECTS OF BOUNDARY LAYER MODELING

Paul E. Long, Jr.
Wilson A. Shaffer

Techniques Development Laboratory
Silver Spring, Md.
May 1975

noaa NATIONAL OCEANIC AND ATMOSPHERIC ADMINISTRATION / National Weather Service

NOAA TECHNICAL MEMORANDA

National Weather Service, Techniques Development Laboratory Series

The primary purpose of the Techniques Development Laboratory of the Office of Systems Development is to translate increases of basic knowledge in meteorology and allied disciplines into improved operating techniques and procedures. To achieve this goal, the laboratory conducts applied research and development aimed at the improvement of diagnostic and prognostic methods for producing weather information. The laboratory performs studies both for the general improvement of prediction methodology used in the National Meteorological Service and for the more effective utilization of weather forecasts by the ultimate user.

NOAA Technical Memoranda in the National Weather Service Techniques Development Laboratory series facilitate rapid distribution of material that may be preliminary in nature and which may be published formally elsewhere at a later date. Publications 1 through 5 are in the former series, Weather Bureau Technical Notes (TN), Techniques Development Laboratory (TDL) Reports; publications 6 through 36 are in the former series, ESSA Technical Memoranda, Weather Bureau Technical Memoranda (WBTM). Beginning with TDL 37, publications are now part of the series NOAA Technical Memoranda, National Weather Service (NWS).

Publications listed below are available from the National Technical Information Service (NTIS), U.S. Department of Commerce, Sills Bldg., 5285 Port Royal Road, Springfield, Va. 22151. Prices vary for paper copy; $1.45 microfiche. Order by accession number, when given, in parentheses at end of each entry.

Weather Bureau Technical Notes

TN 10 TDL 1 Objective Prediction of Daily Surface Temperature. William H. Klein, Curtis W. Crockett, and Carlos R. Dunn, September 1965. (PB-168-590)

TN 11 TDL 2 Hurricane Cindy Galveston Bay Tides. N. A. Pore, A. T. Angelo, and J. G. Taylor, September 1965. (PB-168-608)

TN 29 TDL 3 Atmospheric Effects on Re-Entry Vehicle Dispersions. Karl R. Johannessen, December 1965. (PB-169-381)

TN 45 TDL 4 A Synoptic Climatology of Winter Precipitation From 700-mb. Lows for the Intermountain Areas of the West. Donald L. Jorgensen, William H. Klein, and August F. Korte, May 1966. (PB-170-635)

TN 47 TDL 5 Hemispheric Specification of Sea Level Pressure From Numerical 700-mb. Height Forecasts. William H. Klein and Billy M. Lewis, June 1966. (PB-173-091)

ESSA Technical Memoranda

WBTM TDL 6 A Fortran Program for the Calculation of Hourly Values of Astronomical Tide and Time and Height of High and Low Water. N. A. Pore and R. A. Cummings, January 1967. (PB-174-660)

WBTM TDL 7 Numerical Experiments Leading to the Design of Optimum Global Meteorological Networks. M. A. Alaka and Frank Lewis, February 1967. (PB-174-497)

WBTM TDL 8 An Experiment in the Use of the Balance Equation in the Tropics. M. A. Alaka, D. T. Rubsam, and G. E. Fisher, March 1967. (PB-174-501)

WBTM TDL 9 A Survey of Studies of Aerological Network Requirements. M. A. Alaka, June 1967. (PB-174-984)

WBTM TDL 10 Objective Determination of Sea Level Pressure From Upper Level Heights. William Klein, Frank Lewis, and John Stackpole, May 1967. (PB-179-949)

WBTM TDL 11 Short Range, Subsynoptic Surface Weather Prediction. H. R. Glahn and D. A. Lowry, July 1967. (PB-175-772)

WBTM TDL 12 Charts Giving Station Precipitation in the Plateau States From 700-Mb. Lows During Winter. Donald L. Jorgensen, August F. Korte, and James A. Bunce, Jr., October 1967. (PB-176-742)

WBTM TDL 13 Interim Report on Sea and Swell Forecasting. N. A. Pore and W. S. Richardson, December 1967. (PB-177-038)

WBTM TDL 14 Meteorological Analysis of 1964-65 ICAO Turbulence Data. DeVer Colson, October 1968. (PB-180-268)

WBTM TDL 15 Prediction of Temperature and Dew Point by Three-Dimensional Trajectories. Ronald M. Reap, October 1968. (PB-180-727)

WBTM TDL 16 Objective Visibility Forecasting Techniques Based on Surface and Tower Observations. Donald M. Gales, October 1968. (PB-180-479)

WBTM TDL 17 Second Interim Report on Sea and Swell Forecasting. N. A. Pore and W. S. Richardson, January 1969. (PB-182-273)

WBTM TDL 18 Conditional Probabilities of Precipitation Amounts in the Conterminous United States. Donald L. Jorgensen, William H. Klein, and Charles F. Roberts, March 1969. (PB-183-144)

WBTM TDL 19 An Operationally Oriented Small-Scale 500-Millibar Height Analysis Program. Harry R. Glahn and George W. Hollenbaugh, March 1969. (PB-184-111)

WBTM TDL 20 A Comparison of Two Methods of Reducing Truncation Error. Robert J. Bermowitz, May 1969. (PB-184-741)

WBTM TDL 21 Automatic Decoding of Hourly Weather Reports. George W. Hollenbaugh, Harry R. Glahn, and Dale A. Lowry, July 1969. (PB-185-806)

WBTM TDL 22 An Operationally Oriented Objective Analysis Program. Harry R. Glahn, George W. Hollenbaugh, and Dale A. Lowry, July 1969. (PB-186-129)

WBTM TDL 23 An Operational Subsynoptic Advection Model. Harry R. Glahn, Dale A. Lowry, and George W. Hollenbaugh, July 1969. (PB-186-389)

WBTM TDL 24 A Lake Erie Storm Surge Forecasting Technique. William S. Richardson and N. Arthur Pore, August 1969. (PB-185-778)

(Continued on inside back cover)

NOAA Technical Memorandum NWS TDL-56

SOME PHYSICAL AND NUMERICAL ASPECTS OF BOUNDARY LAYER MODELING

Paul E. Long, Jr.
Wilson A. Shaffer

Techniques Development Laboratory
Silver Spring, Md.
May 1975

UNITED STATES
DEPARTMENT OF COMMERCE
Rogers C. B. Morton, Secretary

NATIONAL OCEANIC AND
ATMOSPHERIC ADMINISTRATION
Robert M. White, Administrator

National Weather
Service
George P. Cressman, Director

CONTENTS

SOME PHYSICAL AND NUMERICAL ASPECTS OF BOUNDARY LAYER MODELING[1]

Paul E. Long, Jr.[2] and Wilson A. Shaffer[3]
Techniques Development Laboratory
National Weather Service, NOAA
Silver Spring, Md. 20910

ABSTRACT. The Techniques Development Laboratory is developing a large scale three-dimensional planetary boundary layer model to predict the temperature, humidity, and wind within the lowest several kilometers of the atmosphere for a period of 24 hr. The output from the model will be used to compute indices for severe storm prediction.

A one-dimensional model which has many of the essential features of the planned three-dimensional model has been run for some time now and is being used to test various formulations of finite-difference schemes, radiation formulations, and suitability of turbulent transfer procedures. The model consists of two basic layers in which are imbedded twelve computational levels. The surface layer uses the Obukhov profile relations with the recent empirical results of Businger et al. (1971) and Webb (1969). The transition layer equations are time dependent and draw their lower boundary conditions from the surface layer relations. The surface temperature is computed by using an energy flux balance. Local radiative heating is included in the temperature calculation above the surface. Many of the features of the one-dimensional model and some comparisons with experimental data are described. A more complete account of the radiation calculations is contained in Shaffer and Long (1973).

This report also describes our recent experiments with two numerical techniques: chapeau functions and cubic splines. These techniques will be used in the solution of the horizontal advective portions of the transiton layer equations.

---

[1]Presented at the Second Conference on Numerical Prediction, 1-4 Oct. 1973, Monterey, California.

[2]Research performed principally while a National Research Council Postdoctoral Associate.

[3]National Research Council Postdoctoral Associate.

I. INTRODUCTION

At the Techniques Development Laboratory of the National Weather Service, we are developing a three-dimensional planetary boundary layer model which will be used to calculate severe storm prediction indices. Our model will make 24-hour predictions of temperature, humidity, and wind from the surface to about two kilometers and will encompass at least the area shown in the small square denoted by "BLM" in figure 1. The horizontal mesh spacing (about 80 km) will be one-half that of the current NMC Limited Area Fine Mesh model (LFM). The current NMC planetary boundary layer model, which computes steady-state winds, has a mesh spacing equal to that of the LFM.

This report will be devoted to two subjects: (1) a general description of the Techniques Development Laboratory's current and future boundary layer models, and (2) a review of some simple numerical experiments using techniques which are evidently fairly new to the field of meteorology and which we plan to use in our boundary layer modeling work. Further details on the one-dimensional model may be found in Shaffer and Long (1973).

Figure 2 shows the spacing of the twelve levels above the contact layer of our current one-dimensional test model. The turbulent diffusion equations are solved by using a transformed system with equal level spacing in the transformed system, although the spacing between the physical levels increases upward. The contact (or surface) layer equations allow us to compute the lower boundary conditions for the time dependent transition layer equations and to compute the surface heat flux required for the prediction of the surface temperature. The LFM or PE models will supply the upper boundary conditions. We have not yet settled the question of whether the model will be limited to the area shown in figure 1 with boundary conditions taken passively from a larger model, or whether we will construct a model of larger total area with a telescoping grid. The utility of telescoping grids will be discussed in section IX.

Although we require an initial soil temperature profile, we are interested only in predicting the temperature at the soil surface and not within the soil. This calculation may be easily handled analytically without soil computational levels.

II. GOVERNING RELATIONS

The prognostic relations for the transition layer are similar to those for "free air" models save for the important terms involving turbulent diffusion and local radiative heating (see Table 1 for symbol definitions). The turbulent diffusion coefficients for heat and humidity are assumed equal, but are not in general equal to the diffusion coefficient for momentum. The four prognostic relations may be reduced to two by using complex variables (2.1-2.4):

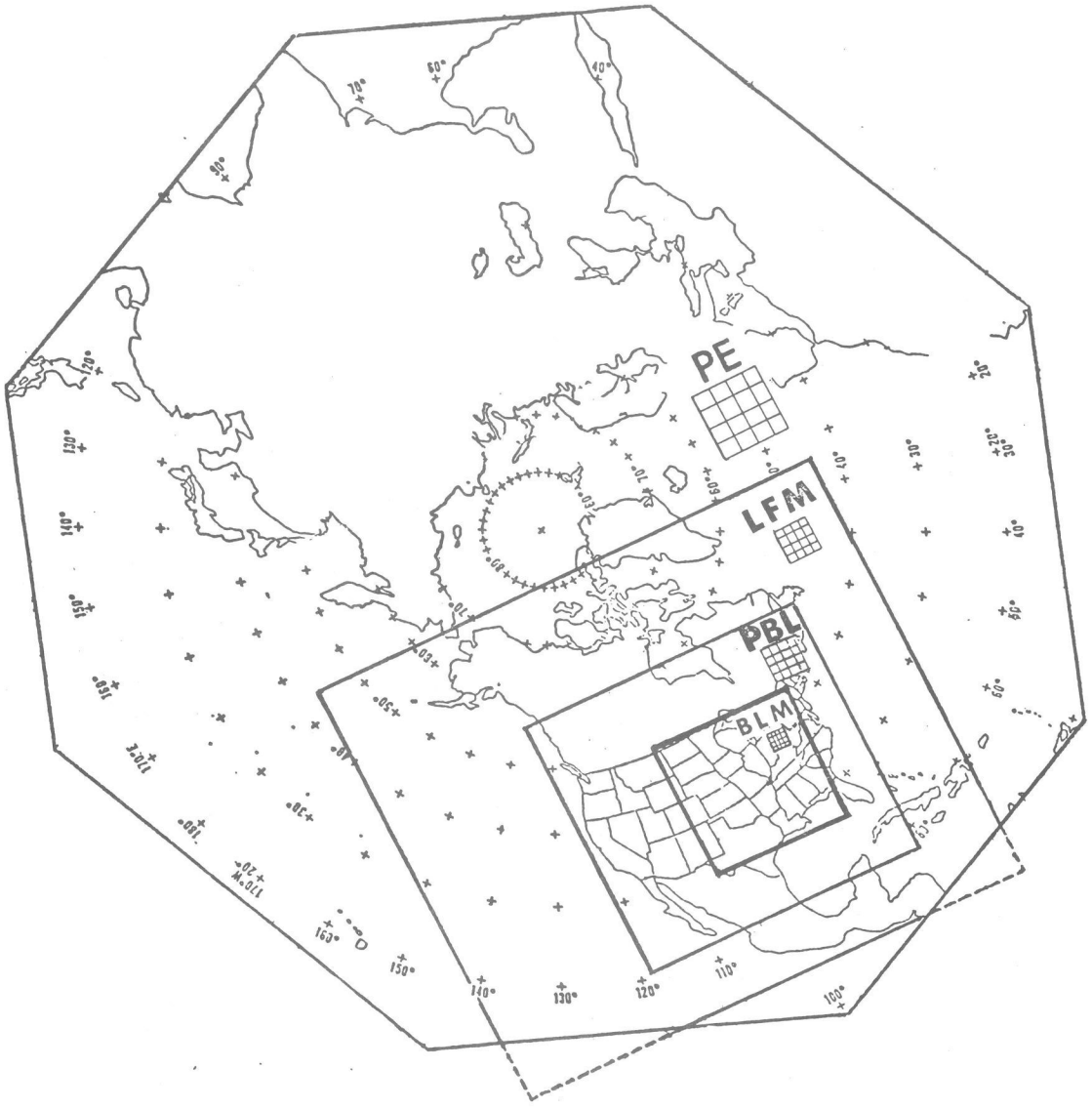

Figure 1.--Forecast areas and grid point spacing of NMC primitive equation (PE), limited area fine-mesh (LFM) and planetary boundary layer (PBL) models. The TDL boundary layer model's (BLM) proposed areal coverage is shown in the inner square.

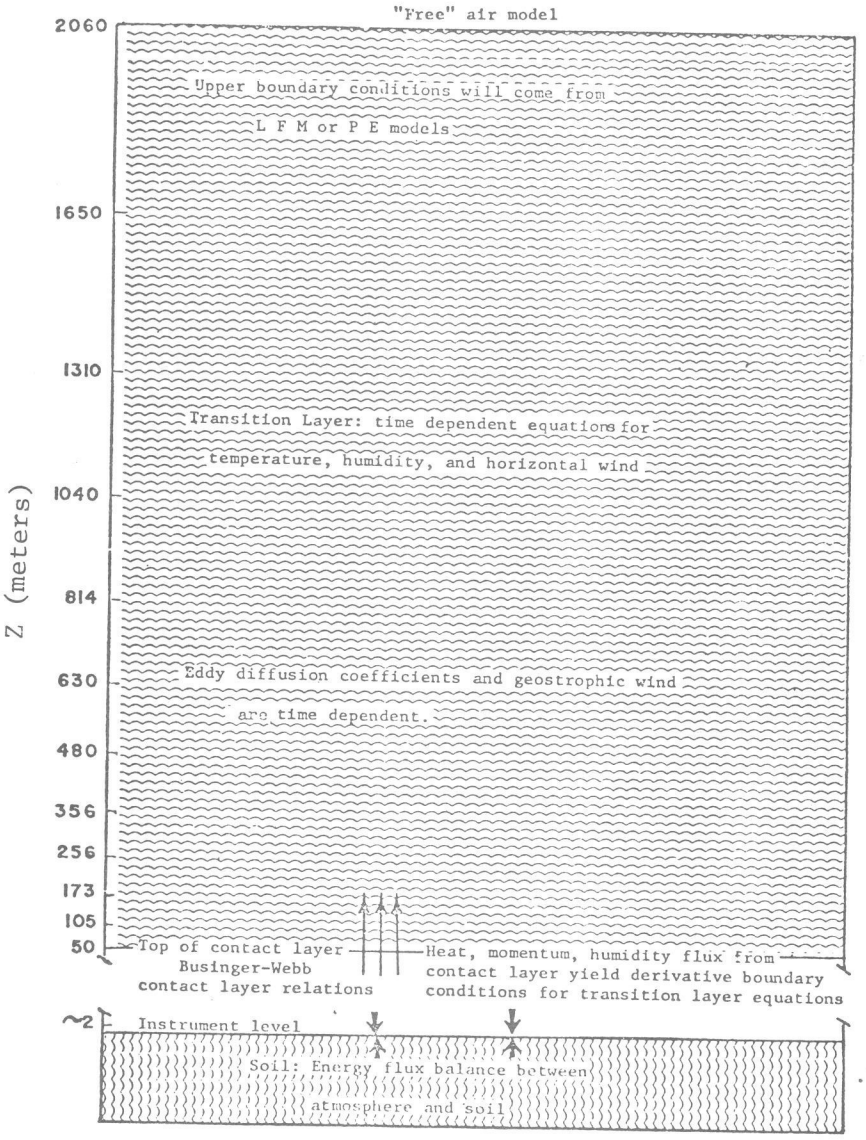

Figure 2.--Vertical schematic of the current one-dimensional boundary layer model. Level spacing increases with height within the transition layer (50 m < z < 2060 m).

Table 1.--List of major symbols

A	stretching parameter for vertical coordinate transformation; a linear combination of chapeau function coefficients
B	linear combination of chapeau function coefficients
e_j	chapeau basis function
f	Coriolis parameter
G	complex geostrophic wind: $u_g + iv_g$; g gravitational acceleration; g(x,t) forcing function in non-linear advection-like equation
H	assumed top of boundary layer model; h assumed top of region where surface relations apply
i	$\sqrt{-1}$
j	finite-difference spatial index
K_M, K_T, K_q	turbulent diffusion coefficients for momentum, temperature and humidity
k	Von Karman constant
L	Obukhov length
n	as in n^{th} iterate; n time step index
P_j	derivative computed using cubic splines
Q_j^n	arbitrary scalar variable at time level n and grid point j; q specific humidity; q_* friction humidity
S	bulk stability parameter
T	complex variable: $\Theta + iq$; t time
U	horizontal wind speed; u east-west wind component; u_g east-west geostrophic wind component; u_* friction speed
V	wind vector; v north-south wind component; v_g north-south geostrophic wind component
W	complex horizontal wind vector: u + iv
Z	vertical coordinate; z_o roughness length; z_i shelter height; Z' transformed vertical coordinate

Table 1. Continued.

α_j	time-dependent chapeau function coefficient for scalar variable Q; recursion relation coefficient
β_j	time-dependent chapeau function coefficient for variable advective velocity; recursion relation coefficient
∇	gradient operator; ΔU, $\Delta\Theta$ difference between values of U and Θ at surface and level z = h; Δt, Δx finite-difference time and space increments
Θ	potential temperature; Θ_* friction temperature
ϕ_m, ϕ_T	Monin-Obukhov universal functions for temperature and wind profiles

$$\frac{\partial \Theta}{\partial t} + \vec{V}\cdot\nabla\Theta = \frac{\partial}{\partial z}\left(K_T \frac{\partial \Theta}{\partial z}\right) + \text{Radiative heating, phase changes}$$

$$\frac{\partial q}{\partial t} + \vec{V}\cdot\nabla q = \frac{\partial}{\partial z}\left(K_q \frac{\partial q}{\partial z}\right)$$

$$\frac{\partial u}{\partial t} + \vec{V}\cdot\nabla u = \frac{\partial}{\partial z}\left(K_m \frac{\partial u}{\partial z}\right) + f\,(v - v_g)$$

$$\frac{\partial v}{\partial t} + \vec{V}\cdot\nabla v = \frac{\partial}{\partial z}\left(K_m \frac{\partial v}{\partial z}\right) + f\,(u_g - u)$$

$$\frac{\partial \tilde{T}}{\partial t} + \vec{V}\cdot\nabla\tilde{T} = \frac{\partial}{\partial z}\left(K_T \frac{\partial \tilde{T}}{\partial z}\right) \qquad (2.1)$$

$$\frac{\partial \tilde{W}}{\partial t} + \vec{V}\cdot\nabla\tilde{W} = \frac{\partial}{\partial z}\left(K_m \frac{\partial \tilde{W}}{\partial z}\right) - if\,(\tilde{W} - \tilde{G}) \qquad (2.2)$$

$$\tilde{T} = \Theta + i\,q \quad ; \quad \tilde{W} = u + i\,v \quad ; \quad \tilde{G} = u_g + i\,v_g \qquad (2.3)$$

$$K_T = K_q \neq K_m \qquad (2.4)$$

The surface layer relations are those suggested by Obukhov (1946),

$$\frac{\partial \Theta}{\partial Z} = \frac{\Theta_*}{kZ}\,\phi_T\left(\frac{Z}{L}\right) \qquad L = \frac{U_*^2\,\overline{\Theta}}{kg\Theta_*}$$

$$\frac{\partial q}{\partial Z} = \frac{q_*}{kZ}\,\phi_q\left(\frac{Z}{L}\right)$$

$$\frac{\partial U}{\partial Z} = \frac{U_*}{kZ}\,\phi_m\left(\frac{Z}{L}\right)$$

The universal functions ϕ_T and ϕ_m have been determined with good precision recently by Businger et al. (1971) and Webb (1970).

For the unstable case:

$$\phi_T = \phi_q = .74 \quad (1 - \gamma_T \frac{Z}{L})^{-1/2}$$

$$\phi_m = (1 - \gamma_m \frac{Z}{L})^{-1/4}$$

For the mildly stable case:

$$\phi_T = \phi_q = .74 + 4.7 \frac{Z}{L}$$

$$\phi_m = 1. + 4.7 \frac{Z}{L}$$

$$\gamma_T = 9 \quad ; \quad \gamma_m = 15 \quad ; \quad k = .35$$

To obtain U_*, Θ_*, q_*, and L, the Businger relationships must first be integrated.

$$\Delta\Theta \equiv \int_{z_i}^{h} dz \frac{\partial\Theta}{\partial Z} = \frac{\Theta_*}{k} [\quad]_\Theta$$

$$\Delta U \equiv \int_{z_o}^{h} dz \frac{\partial U}{\partial Z} = \frac{U_*}{k} [\quad]_u$$

$$[\quad]_\Theta = .74 \ln \left\{ \frac{(\sqrt{1 - \gamma_T \frac{h}{L}} - 1)(\sqrt{1 - \gamma_T \frac{Z_i}{L}} + 1)}{(\sqrt{1 - \gamma_T \frac{h}{L}} + 1)(\sqrt{1 - \gamma_T \frac{Z_i}{L}} - 1)} \right\}$$

$$[\quad]_u = \ln \left\{ \frac{\left[\left(1 - \gamma_m \frac{h}{L}\right)^{1/4} - 1\right]\left[1 + \left(1 - \gamma_m \frac{Z_o}{L}\right)^{1/4}\right]}{\left[1 + \left(1 - \gamma_m \frac{h}{L}\right)^{1/4}\right]\left[\left(1 - \gamma_m \frac{Z_o}{L}\right)^{1/4} - 1\right]} \right\}$$

$$+ 2 \left[\tan^{-1}\left(1 - \gamma_m \frac{h}{L}\right)^{1/4} - \tan^{-1}\left(1 - \gamma_m \frac{Z_o}{L}\right)^{1/4}\right]$$

It will be noted that where L>0, Businger's relationships are more easily integrated than those of Dyer (1967). For instance, Krishna's (1968) boundary layer model which used Dyer's ϕ's required a numerical integration each time the surface relations were invoked.

Let us suppose that the wind velocity, temperature, and specific humidity are known at the bottom of the transition layer (Z=h) and all but the wind are known at the instrument level, Z_i. This information is sufficient to determine U_*, Θ_*, and L, and also

$$\frac{\partial \Theta}{\partial Z}_h, \quad \frac{\partial q}{\partial Z}_h, \text{ and } \quad \frac{\partial U}{\partial Z}_h,$$

the derivatives of temperature, humidity, and wind speed at the top of the surface layer. Since the surface layer eddy diffusion coefficients are given by

$$K_T(Z) = kU_*Z/\phi_T(Z/L)$$

and

$$K_m(Z) = kU_*Z/\phi_m(Z/L),$$

both $K_T(h)$, $K_m(h)$ and $(\partial K_T/\partial Z)_h$, $(\partial K_m/\partial Z)_h$ are readily calculated. The derivatives of temperature, humidity, and wind velocity supply the lower boundary conditions for the parabolic transition layer equations. We use the O'Brien (1970) cubic diffusion coefficient profile in the transition layer as a temporary computational expedient; although the profile has a K maximum within the transition layer above which K decreases as one may reasonably expect, local values of K are uninfluenced by local stability. On the other hand, our experience shows that diffusion coefficients which depend upon stability (Richardson numbers) often create subtle numerical instabilities which can grow beyond control. A sure curative is the reduction of the time step used in the numerical marching process, but we feel that we must use a time step of about thirty minutes to keep the three-dimensional model economically feasible.

The integrated profile relations along with the defining relation for L, the Obukhov length, contain Θ_*, U_*, and L as unknowns. We have an efficient solution for this system: we eliminate the variables U_* and Θ_* by defining a new parameter, S, given by

$$S \equiv \frac{\Delta U^2 \, \bar{\Theta}}{g \Delta \Theta}$$

which allows us to combine the integrated profile relations as follows,

$$L = \frac{[\quad]_\Theta}{[\quad]_u^2} \, S.$$

The bracketed terms depend upon the Obukhov length only. In the unstable case, this relation creates a rapidly converging sequence,

$$L^{(n+1)} = \frac{[\ L^{(n)}\ ]_\Theta}{[\ L^{(n)}\ ]_u^2}\ S$$

If the initial value for L is taken to be the nearly-neutral value, then the rate of convergence increases with increasing $|S|$. For practical purposes we have found three or four iterations to be sufficient.

When the surface layer is mildly stable, no iteration is required; one simply solves the quadratic,

$$a\ L^2 + bL + c = 0\ , \text{ where}$$

$$a = \ln^2 \frac{h}{Z_o};\ b = 9.4\ (h - Z_o)\ \ln \frac{h}{Z_o} - .74S \ln \frac{h}{Z_i}$$

$$c = [4.7(h-Z_o)]^2 - 4.7\ (h-Z_i)S$$

$$L = \frac{-b + \sqrt{b^2 - 4ac}}{2a}\ ,$$ in which only the (+) solution has physical meaning.

Because of their similar structure, S and L must have the same algebraic sign, a property which cannot be guaranteed during strong stability (small + S). In addition, Webb (1970) has suggested a change in the log + linear integrated profile relation whenever Z>L. For $\frac{Z}{L} > 1$, he suggested that ϕ_T and ϕ_T become equal to their values at Z=L. For the Businger stable profile this means

$$\left.\begin{aligned} \phi_T &= .74 + 4.7 = 5.44 \\ \phi_m &= 1. + 4.7 = 5.7 \end{aligned}\right\}\ Z \geq L$$

To calculate the bracketed terms for very stable conditions, we must integrate the unmodified Businger relations up to Z=L and then to h using Webb's profile. The result is

$$[\qquad]_\Theta = .74 \ln \frac{L}{Z_i} + \frac{4.7}{L}\ (L - Z_i) + 5.44 \ln \frac{h}{L}$$

$$[\qquad]_u = \ln \frac{L}{Z_o} + \frac{4.7}{L}\ (L - Z_o) + 5.7 \ln \frac{h}{L}$$

As with the unstable case, L must be found by iteration.

After L is computed, Θ_*, U_*, q_*, and all of the required derivatives follow easily. Table 2 contains a summary of the contact layer relations.

Table 2: Summary of Surface Layer Equations

1. From $\Delta\Theta$, ΔU form

$$S = \frac{\Delta U^2 \overline{\Theta}}{g \Delta \Theta} \quad . \quad \overline{\Theta} \text{ is average boundary layer temperature.}$$

2. If $\Delta\Theta < 0$ or if highly stable ($h > L$), iterate:

$$L^{(n+1)} = \frac{[\ L^{(n)}]_{\Theta}}{[\ L^{(n)}]_u^2} \quad S.$$

3. If mildly stable, quadratic relation for L

4. After $L^{(n)}$ converges, compute

$$\Theta_* = \frac{k\Delta\Theta}{[\ ]_{\Theta}} \quad ; \quad U_* = \frac{k\Delta U}{[\ ]_u}$$

$$q_* = \frac{\Delta q}{\Delta\Theta}\,\Theta_* \quad ; \left(\frac{\partial\Theta}{\partial Z}\right)_h = \frac{\Theta_*}{kh}\,\phi_T\left(\frac{h}{L}\right)$$

$$\left(\frac{\partial q}{\partial Z}\right)_h = \frac{q_*}{kh}\,\phi_T\left(\frac{h}{L}\right) \quad ; \quad \left(\frac{\partial u}{\partial Z}\right)_h = \frac{U_*}{kh}\,\phi_m\left(\frac{h}{L}\right) \cos\alpha$$

$$\left(\frac{\partial v}{\partial Z}\right)_h = \frac{U_*}{kh}\,\phi_m\left(\frac{h}{L}\right) \sin\alpha$$

$$K_T\ (Z \leq h) = \frac{kU_*Z}{\phi_T\left(\frac{Z}{L}\right)} \quad ; \quad K_m\ (Z \leq h) = \frac{kU_*Z}{\phi_m\left(\frac{Z}{L}\right)}$$

$$K\ (h<Z<H) = K_h + \left(\frac{Z-H}{H-h}\right)^2 \left\{ K_h - K_H + (Z-h)\left[\left(\frac{\partial K}{\partial Z}\right)_h + \frac{2\,(K_h - K_H)}{H-h} \right] \right\}$$

α = current wind vector angle

III. NUMERICAL SOLUTION OF THE TRANSITION LAYER EQUATIONS

We investigated a number of finite-difference schemes which have been used in various boundary layer models and found most of them to be unsuited for our purposes (Long 1973). However, the implicit Crank-Nicolson scheme generally allowed time steps that are only limited by the amount of time the boundary conditions may be held fixed without degrading the solution.

The Crank-Nicolson scheme may be applied to the expanding system of levels by using a transformed Z' coordinate system,

$$Z' = A \ln \left[1 + \frac{Z - h}{A}\right] + h.$$

Although ΔZ increases with height, $\Delta Z'$ is constant and set equal to 50 m. The temperature diffusion equation in the transformed system is

$$\frac{d\Theta}{dt} = g(Z) \frac{\partial}{\partial Z'} \left[g(Z) \frac{\partial \Theta}{\partial Z'} \right], \qquad g(Z) \equiv \frac{dZ'}{dZ}$$

which becomes in finite-difference form,

$$\frac{\Theta_j^{n+1} - \Theta_j^n}{\Delta t} = g_j \left\{ g_{j-1/2} K^n_{j-1/2} \Theta^{n+1}_{j-1} - \left(g_{j-1/2} K^n_{j-1/2} + g_{j+1/2} K^n_{j+1/2} \right) \Theta^{n+1}_j \right.$$

$$\left. - g_{j+1/2} K^n_{j+1/2} \Theta^{n+1}_{j+1} + g_{j-1/2} K^n_{j-1/2} \Theta^n_{j-1} - \left(g_{j-1/2} K^n_{j-1/2} + g_{j+1/2} K^n_{j+1/2} \right) \Theta^n_j \right.$$

$$\left. - g_{j+1/2} K_{j+1/2} \Theta^n_{j+1} \right\} \Big/ 2(\Delta Z')^2.$$

IV. SEQUENCE OF OPERATIONS

Figure 3 shows the sequence in which the operations are carried out in the one-dimensional model. (1) Profiles of temperature, humidity, and geostrophic wind must given initially. (2) If not measured, initial horizontal winds are computed using similarity relations in the surface layer and a numerical solution to the generalized Ekman equation

$$\frac{d}{dZ} \left(K_m(Z) \frac{d\widetilde{W}}{dZ} \right) - \text{if } (\widetilde{W} - \widetilde{G}) = 0$$

in the transition layer. (3) The calculation of U_*, Θ_*, and L permit (4) the computation of

$$\frac{\partial U}{\partial Z}, \frac{\partial \Theta}{\partial Z}, \frac{\partial q}{\partial Z}, K_T, K'_T, K_m, \text{ and } K'_m.$$

SOLUTION OF THE PROGNOSTIC EQUATIONS

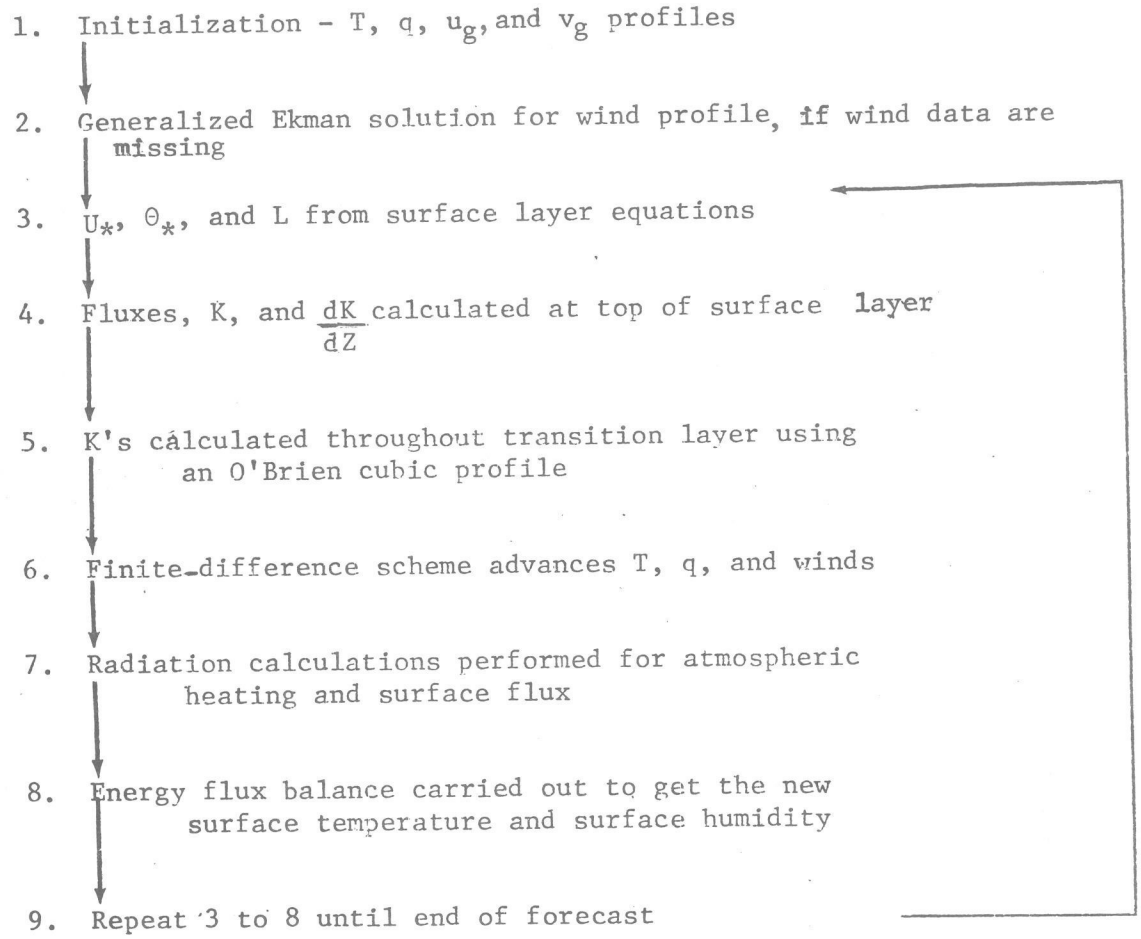

Figure 3.--Summary of steps required for the solution of the boundary layer model.

at the top of the surface layer. (5) From O'Brien's cubic profile relation and (4), K_T and K_m can be calculated throughout the transition layer. (6) The Crank-Nicolson finite-difference scheme advances the solution of the temperature, wind, and humidity equations one time step, Δt. The lower boundary condition requires the slopes of Θ, q and u, v at the bottom of the transition layer be set equal to the values in (4). This means all the Θ, q, u, v (including the level at Z=h) will be marched. (7) A radiative flux divergence adds to the local heating and cooling rates. A surface radiation flux is required for the surface energy balance. (8) The contact layer relations and the surface radiation flux are used in a surface energy flux balance to compute a new surface temperature. (9) Steps (3)-(8) are repeated until the forecast is completed.

V. RESULTS OF THE CALCULATIONS

Some comparisons between the model's predictions and the data from Wangara, Australia (Clarke, et al. 1971) and O'Neill, Nebraska (Lettau and Davidson, 1957) will be shown in the following figures. The top portion of figure 4, for Wangara experiment day number 39, shows the 2-m temperatures. The observed and predicted values are in almost perfect agreement during the night and deviate by at most 1°C during the day.

Figure 4 also shows the calculated and observed surface wind. The simultaneous wind measurements were taken from observation points separated by about 10 km. There is a great deal of scatter during the early morning hours with a wind maximum occuring at about 9:00 AM and a secondary maximum at 1:00 PM. Although the secondary maximum is not captured by the model at all, the primary maximum is fairly well handled.

Figure 5 shows the temperature wave for heights of 200, 400, and 1000 meters. The predicted values improve as one approaches the surface where the advective effects (obviously not handled by a one-dimensional model) are presumably diminished.

There is good agreement between predicted and measured values for the surface net radiation and soil heat flux as shown in figure 6. The measurements were taken during observed changing cloud conditions for which we have made provision in the model.

The published values of the geostrophic winds include large errors and make accurate predicted values of wind high in the transition layer almost impossible. This is shown in figure 7. Fairly strong deviations occur above 400 meters.

Figure 8 shows the effect of neglecting local radiative heating at four levels within the model. The effect is profound at 105 meters and is not insignificant even at 256 meters. We were surprised by these results.

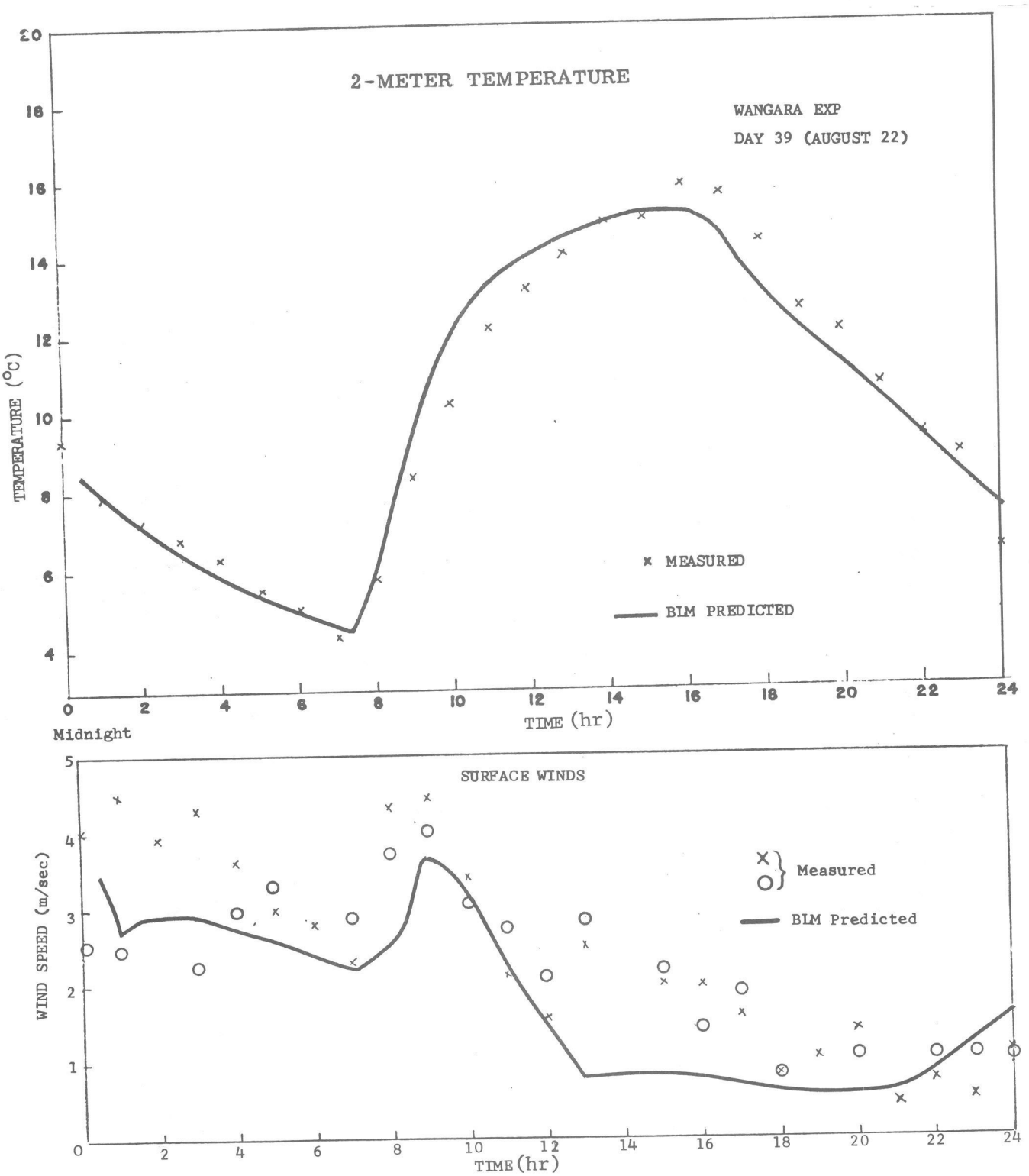

Figure 4.--Two-meter temperature and three-meter winds for the Wangara experiment, day 39. Solid curves denote model-computed values. Crosses and circles are measured values spanning a period of 24 hours.

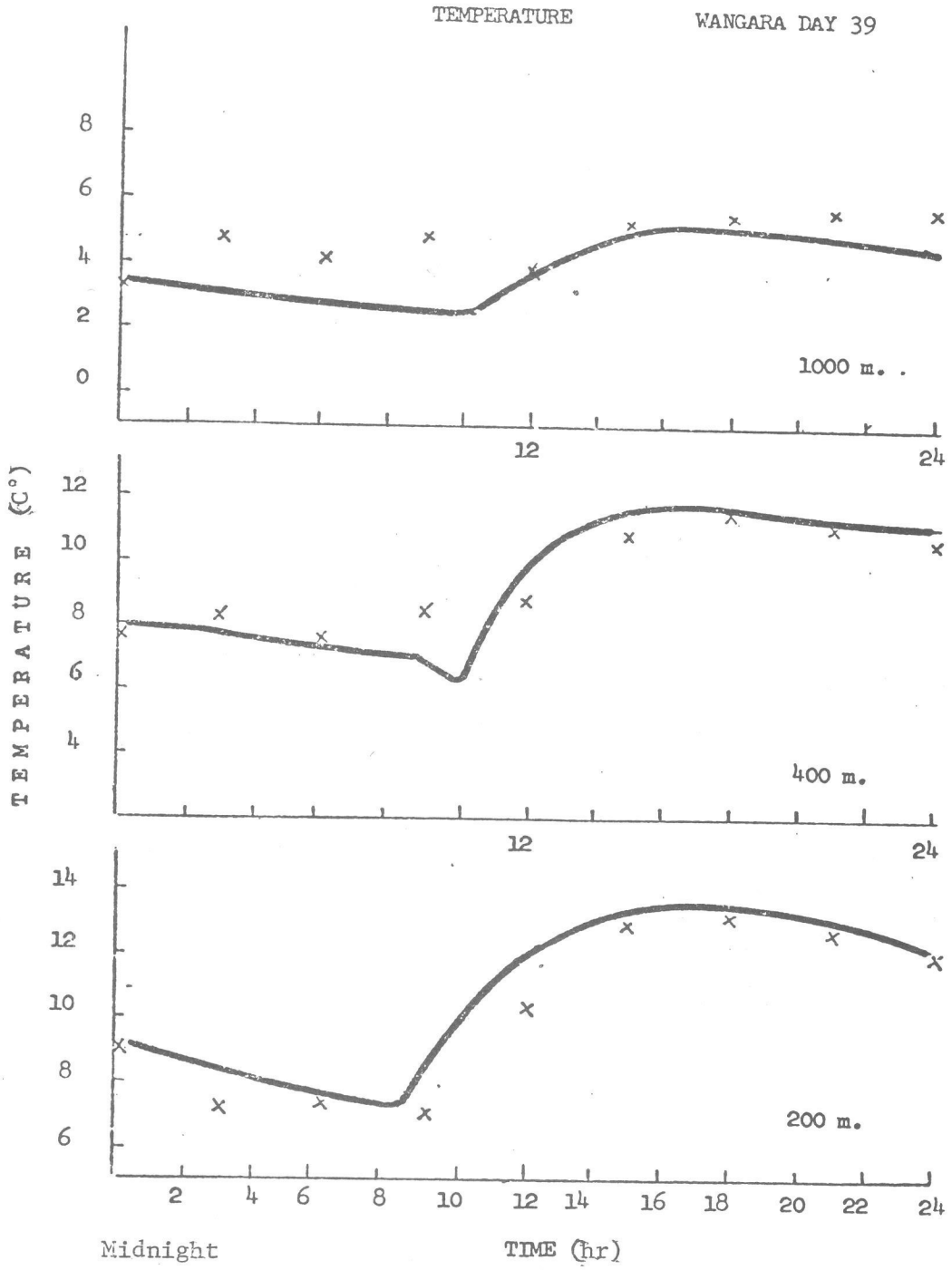

Figure 5.--Computed (solid curve) and measured (crosses) temperatures at heights of 200, 400, and 1000 meters for Wangara day 39.

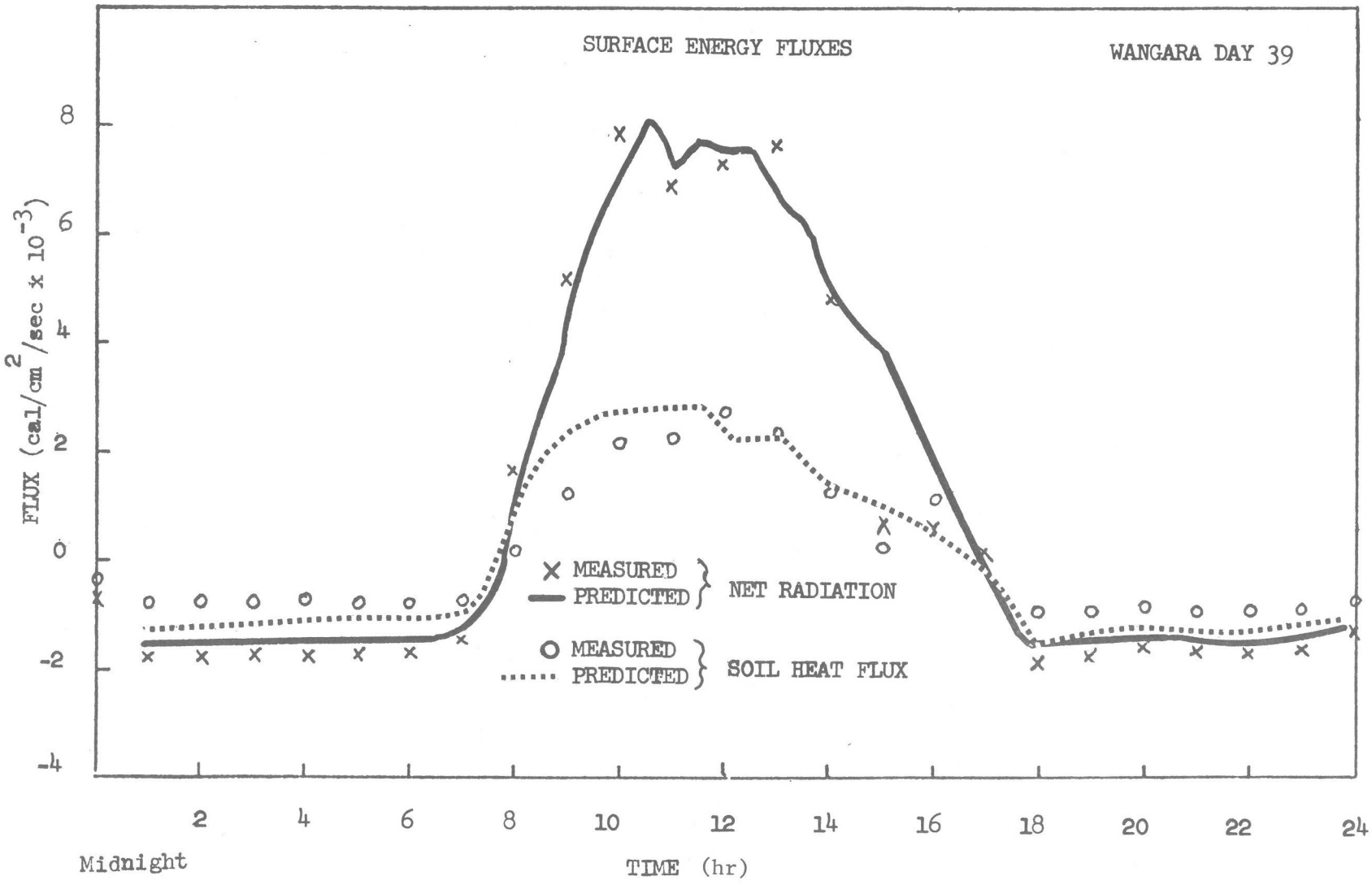

Figure 6.--Surface net radiation (solid curve) and soil heat (dotted curve) fluxes for Wangara day 39. The small dip in plateau of net radiation curve is caused by the intrusion of cloud cover.

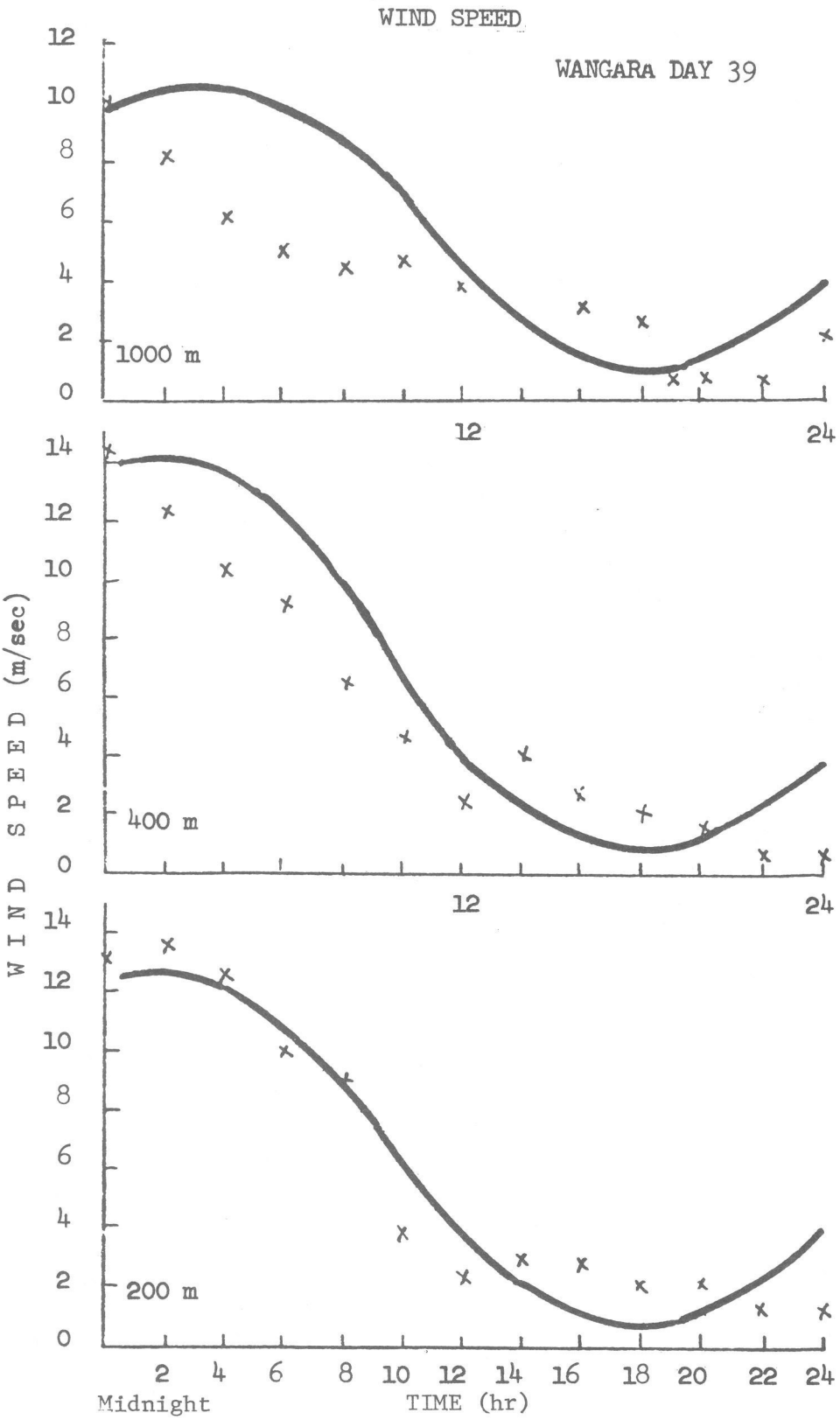

Figure 7.--Same as figure 5 except wind replaces temperature.

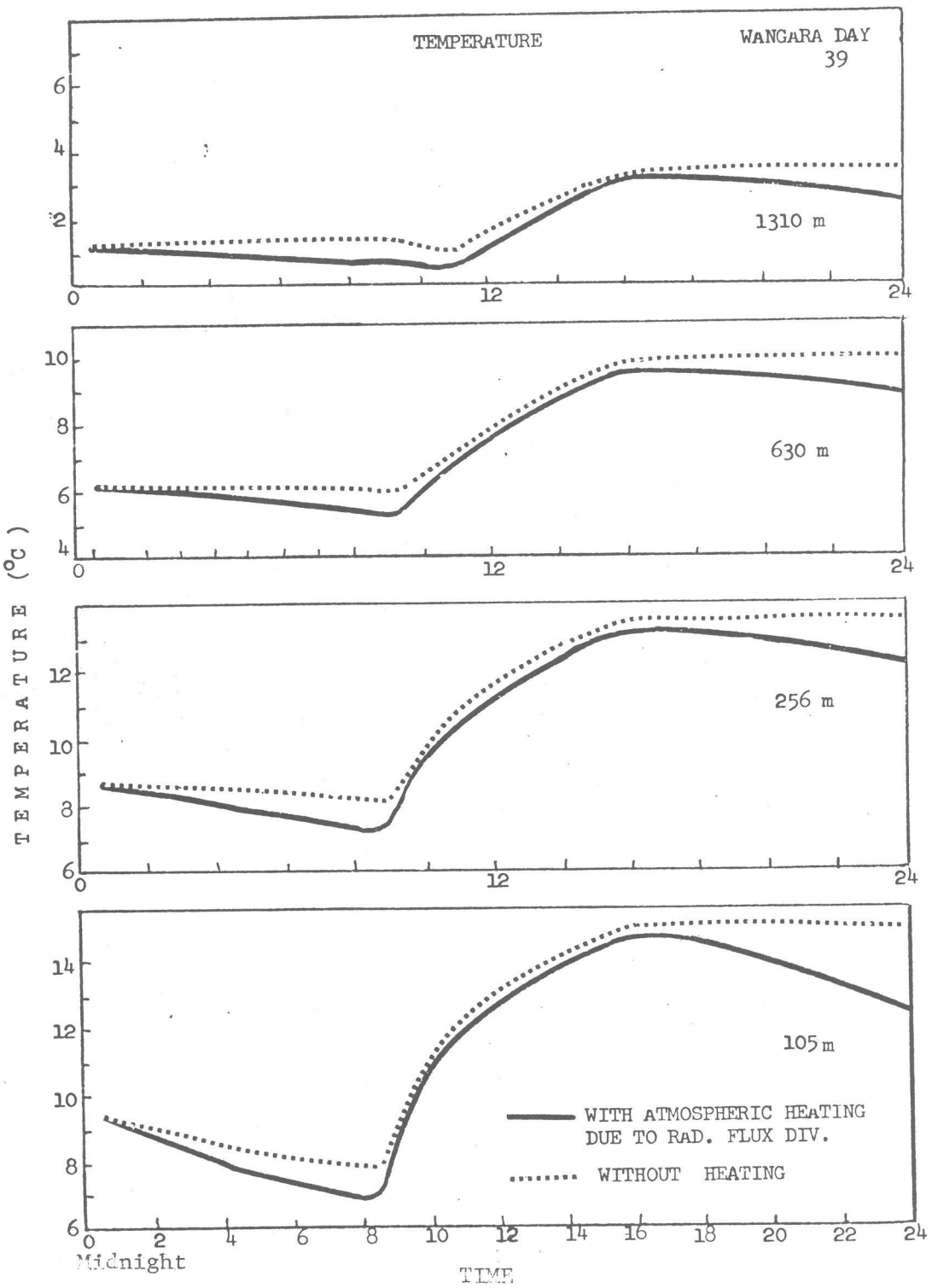

Figure 8.--Predicted temperatures for Wangara day 39 at heights 105, 256, 630, and 1310 meters with (solid curves) and without (dotted curves) atmospheric heating due to radiative flux divergence. Without radiative effects, temperatures are not sufficiently depressed at night.

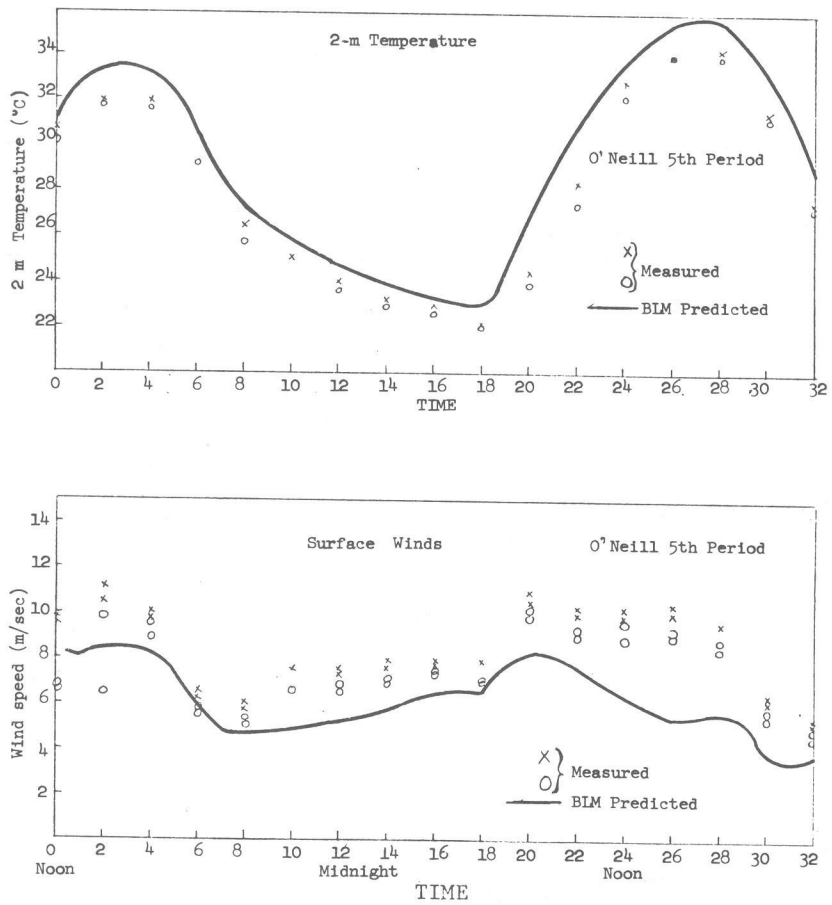

Figure 9.--Same as figure 4 but for the O'Neill 5th period.

There is good agreement between the calculated and measured 2-meter temperatures for the O'Neill 5th period, shown in figure 9. The correspondence is fair for the surface winds.

VI. SOME RECENT EXPERIMENTS WITH NUMERICAL TECHNIQUES

We have analyzed and experimented with a number of finite-difference diffusion and advection schemes. A summary of the properties of the diffusion schemes may be found in Long (1973).

In an effort to extend the integrating time step of the difference schemes without inducing computational instability, we devised some new implicit advection schemes with the idea of applying the technique of "splitting" (extensive Soviet literature now exists on the subject of splitting; a good text is Yanenko 1971). Although the schemes usually had excellent stability properties, their truncation errors were often as great or greater than standard second-order explicit schemes.

Dr. James Bradley of Drexel University recently suggested the use of spline and chapeau functions for solving time-dependent problems. We shall show some results of our investigation in section IX.

VII. CHAPEAU FUNCTIONS

Graphs of chapeau functions look like peaked hats; hence their name. For a one-dimensional array of N gridpoints there are N such chapeau basis functions defined by

$$
\begin{aligned}
e_j\ (x) &\equiv \frac{x - x_{j-1}}{x_j - x_{j-1}}, \quad x \in [x_{j-1},\ x_j] \\
e_j\ (x) &\equiv \frac{x_{j+1} - x}{x_{j+1} - x_j}, \quad x \in [x_j,\ x_{j+1}] \\
e_j\ (x) &\equiv 0, \qquad\quad x \in [x_{j-1},\ x_{j+1}]
\end{aligned}
\tag{7.1}
$$

Figure 10 shows such an array.

As a test problem we shall solve the advection equation,

$$\frac{\partial Q}{\partial t} + U \frac{\partial Q}{\partial x} = 0;\ U = \text{constant} \tag{7.2}$$

by approximating Q (x, t) in terms of the chapeau basis functions,

$$Q\ (x,\ t) = \sum_j \alpha_j\ (t)\ e_j\ (x). \tag{7.3}$$

If Q (x, t) is defined at N gridpoints, then the coefficients, $\alpha_j(t)$, are simply equal to Q (x_j, t). When (7.3) is substituted into (7.2) and the

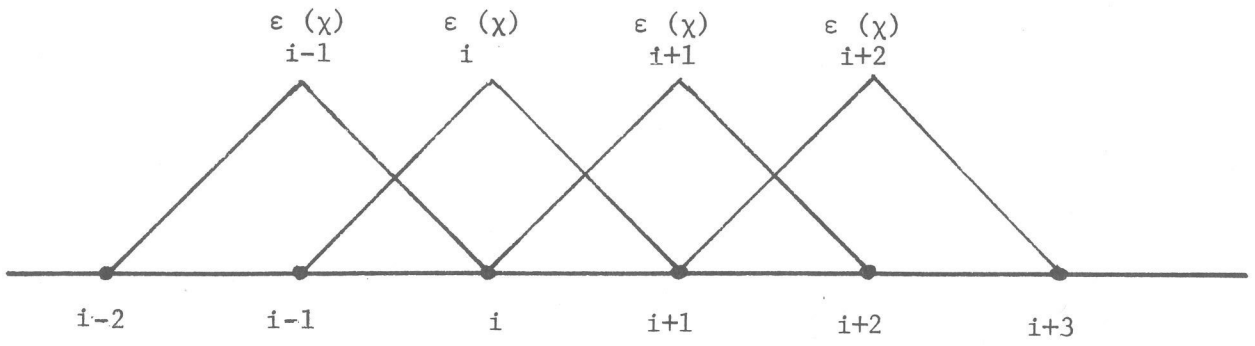

Figure 10.--Portion of a one-dimensional grid showing piecewise linear chapeau basis functions.

result is integrated over (Galerkin's method) by $e_k(x)$, the relation becomes

$$1/6\,\frac{d}{dt}\,(\alpha_{j-1} + 4\,\alpha_j + \alpha_{j+1}) + \frac{U\Delta t}{2\Delta x}\,(\alpha_{j+1} - \alpha_{j-1}) \equiv \frac{dA}{dt} + B = 0. \qquad (7.4)$$

$$\left.\begin{aligned} A &\equiv 1/6\,(\alpha_{j-1} + 4\,\alpha_j + \alpha_{j+1}) \\ B &\equiv \frac{U\Delta t}{2\Delta x}\,(\alpha_{j+1} - \alpha_{j-1}) \end{aligned}\right\}. \qquad (7.5)$$

There are a number of plausible ways of integrating the difference-differential equation (7.4), three of which are displayed below:

1) Two level:

$$\frac{A^{n+1} - A^n}{\Delta t} + 1/2\,(B^n + B^{n+1}) = 0 \qquad (7.6)$$

which is stable regardless of Δt,

2) Three level: (7.7)

$$\frac{A^{n+1} - A^{n-1}}{2\Delta t} + B^n = 0$$

which is stable provided $\frac{U\Delta t}{\Delta x} \leq 1/2$, and

3) Three level:

$$\frac{A^{n+1} - A^{n-1}}{2\Delta t} + 1/6\,(B^{n+1} + 4\,B^n + B^{n-1}) = 0 \qquad (7.8)$$

which is stable provided $\frac{U\Delta t}{\Delta x} \leq 1$.

The superscripts refer to the time level $n = t/\Delta t$.

When the advection velocity is variable, the analogous equation is more complicated in detail but is fundamentally the same as (7.5):

$$\frac{\partial Q}{\partial t} + u\,(x, t)\,\frac{\partial Q}{\partial x} = 0$$

$$\left.\begin{aligned} Q\,(x, t) &= \sum_j \alpha_j\,(t)\,e_j\,(x) \\ u\,(x, t) &= \sum_j \beta_j\,(t)\,e_j\,(x) \end{aligned}\right\}$$

$$\frac{dA}{dt} + B = 0$$

$$A \equiv 1/6\,(\alpha_{j-1} + 4\,\alpha_j + \alpha_{j+1})$$

$$B \equiv 1/6\Delta x \left[(2\beta_j + \beta_{j+1})\ \alpha_{j+1} \right.$$

$$- (\beta_{j+1} - \beta_{j-1})\ \alpha_j$$

$$\left. - (2\beta_j + \beta_{j-1})\ \alpha_{j-1} \right] .$$

VIII. CUBIC SPLINES

The concept behind the use of cubic splines is simple indeed. The idea is to take the standard leap-frog scheme

$$\frac{Q_j^{n+1} - Q_j^{n-1}}{2\Delta t} + \frac{U}{2\Delta x} \left(Q_{j+1}^n - Q_{j-1}^n \right) = 0$$

and to replace the spatial derivative (of second-order accuracy) by a cubic spline derivative of greater accuracy, P_j^n,

$$\frac{Q_j^{n+1} - Q_j^{n-1}}{2\Delta t} + P_j^n = 0 .$$

The spline derivative at a point is linked with its neighbors by the relation (proved in Ahlberg, et al. 1965)

$$A_j\ P_{j-1}^n + B_j P_j^n + C_j\ P_{j+1}^n = D_j$$

in which

$$\left.\begin{aligned} A_j &= \frac{x_{j+1} - x_j}{x_{j+1} - x_{j-1}} \quad ; \quad B_j = 2 \quad ; \quad C_j = 1 - A_j \\ D_j &= \frac{3A_j (Q_j^n - Q_{j-1}^n)}{x_j - x_{j-1}} + \frac{3C_j\ (Q_{j+1}^n - Q_j^n)}{x_{j+1} - x_j} \end{aligned}\right\} .$$

As with the chapeau function technique, the system of equations forms a 3-band (or tridiagonal) matrix system which is solved by using the recursion relations

$$P_{j+1}^n = \alpha_j P_j^n + \beta_j$$

$$\alpha_j = - A_{j+1}/E_j$$

$$\beta_j = (D_{j+1} - \beta_{j+1}\ C_{j+1})/E_j$$

$$E_j = B_{j+1} + \alpha_{j+1}\ C_{j+1}$$

In the above, x_j is the coordinate of grid point j. A_j, B_j, C_j, and E_j are functions of the coordinates and have only to be computed once. If the boundary conditions are fixed throughout the time of computation, α_j remains constant, also. β_j must be computed at each time step.

One of the useful properties of spline derivatives (besides their higher order accuracy) is the freedom to specify arbitrarily the location of grid points permitting, if one wishes, a succession of telescoping grids. A fine resolution grid is used in the area of greater interest which is surrounded by a coarse grid in the area of lesser interest. A telescoping grid allows the boundaries to be pushed far enough away from the forecast area of primary interest that their importance is presumably greatly diminished. This is not to say that one is completely rid of the problems which occur at the interface of two differing mesh densities, but the freedom of the spline relations allows us to mitigate them somewhat. The problem of "nesting" a fine mesh grid passively within a coarse mesh region which is run separately is thereby avoided.

Considerable literature has developed on the use of splines as interpolating tools, but there has been apparently no application of splines to the solution of the predictive equations of meteorology until recently (Price and MacPherson 1973). In the process of interpolation, splines tend to produce a curve relatively free of wrinkles. If one defines a wrinkle mathematically as the second derivative of a function, then, under fairly generous conditions, one can prove that if S(x) is the spline interpolation to the known function f(x), then the integral

$$\int dx \left| f''(x) - S''(x) \right|^2$$

is minimized. Of course, we are only concerned with evaluating the derivatives of the splines at gridpoints; the actual interpolating formulas are of no particular use to us.

One potential drawback to the use of the cubic spline is its non-local nature; that is, a derivative at a particular grid point necessarily involves all of the other grid points (to a diminished degree). This means that a function that undergoes a sharp change or is discontinuous at a particular point is likely to influence strongly the spline derivatives at other points. Although we found that discontinuities in the initial function were handled badly, continuous functions with discontinuous derivatives were much more successfully treated by splines than by the second-order leap-frog scheme.

Another caveat is necessary: replacing spatial by spline derivatives does not guarantee a stable difference scheme. The cubic spline solution to the linear equation

$$\frac{\partial Q}{\partial t} + \frac{U \partial Q}{\partial x} = 0$$

becomes unstable whenever the Courant number, $U \frac{\Delta t}{\Delta x}$, exceeds a number somewhere between 0.55-0.60 as compared to a Courant limit of unity for the second-order leap-frog scheme. The reduction of the allowable Courant number is

not surprising. If the spatial derivatives of the leap-frog scheme were replaced by exact spatial derivatives, then the upper limit would be reduced further to $1/\pi$.

We also found that we must be careful with the non-linear equations expressed as

$$\frac{\partial u}{\partial t} + u\frac{\partial u}{\partial x} = g\ (x,\ t)$$

Use of the spline derivative leads to very poor, generally distinctly unstable results. However, rewriting the equation in its algebraically equivalent flux-form and then using spline derivatives of

$$\frac{\partial u}{\partial t} + \frac{1}{2}\frac{\partial u^2}{\partial x} = g\ (x,\ t)$$

restores stability for Courant numbers up to (at least) 0.4. Apparently conservative forms are required.

IX. NUMERICAL EXPERIMENTS

All of the experiments in this section were performed with Gaussian initial states centered at $x = 10\Delta x$:

$$Q\ (x,\ t=0) = \exp\ [\ -\ \frac{(x-10)^2}{w^2}]\ ;\ \Delta x = 1 \qquad (9.1)$$

with half-widths, w, of $2\Delta x$. In (9.1), $Q\ (x,\ t=0)$ is reduced by a factor of $1/e$ a distance w from its center.

The two equations to be studied are: $\frac{\partial Q}{\partial t} + U\frac{\partial Q}{\partial x} = 0$

and $\frac{\partial u}{\partial t} + \frac{1}{2}\frac{\partial u^2}{\partial x} = g\ (x,\ t).$

The forcing function $g\ (x,\ t)$ is chosen so the Gaussian propagates undistorted with a speed of unity (one grid point per unit time) for both the linear and non-linear equations. Thus,

$$g\ (x,\ t) = (f - U)\frac{\partial f}{\partial q}$$

$$f\ (q) = \exp\ (-q^2)$$

$$q = (x - Ut + 10)/w \quad ;\ U = \Delta x = 1.$$

The terminal point is $x = 40\Delta x$ regardless of the time step.

Figure 11 shows the result of a numerical simulation of the linear equation using the chapeau two-level scheme (7.6) and the Crank-Nicolson implicit advection scheme,

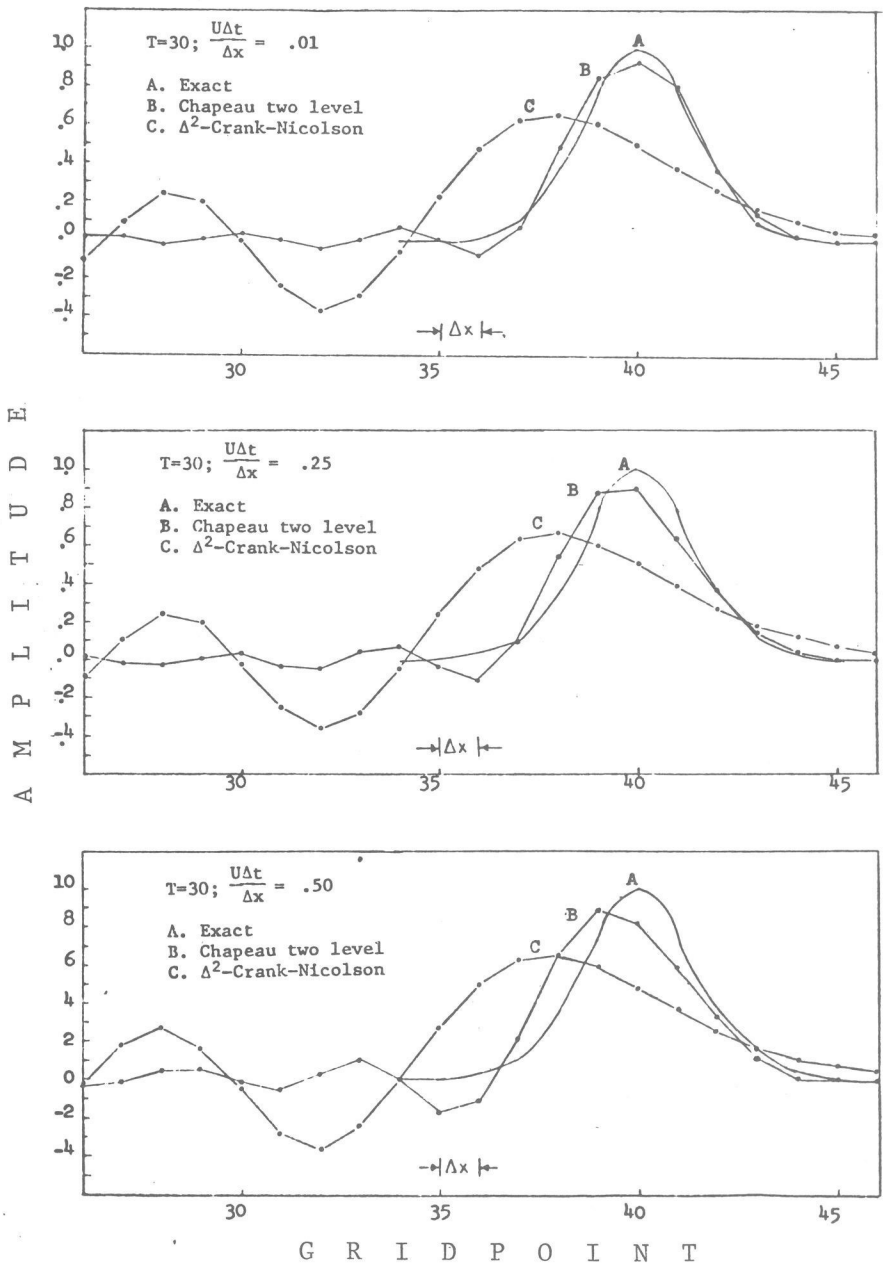

Figure 11.--Comparison of exact (curve A), chapeau two-level (curve B), and Crank-Nicolson (curve C) solutions of the linear advection equation for various Courant numbers. See text for details.

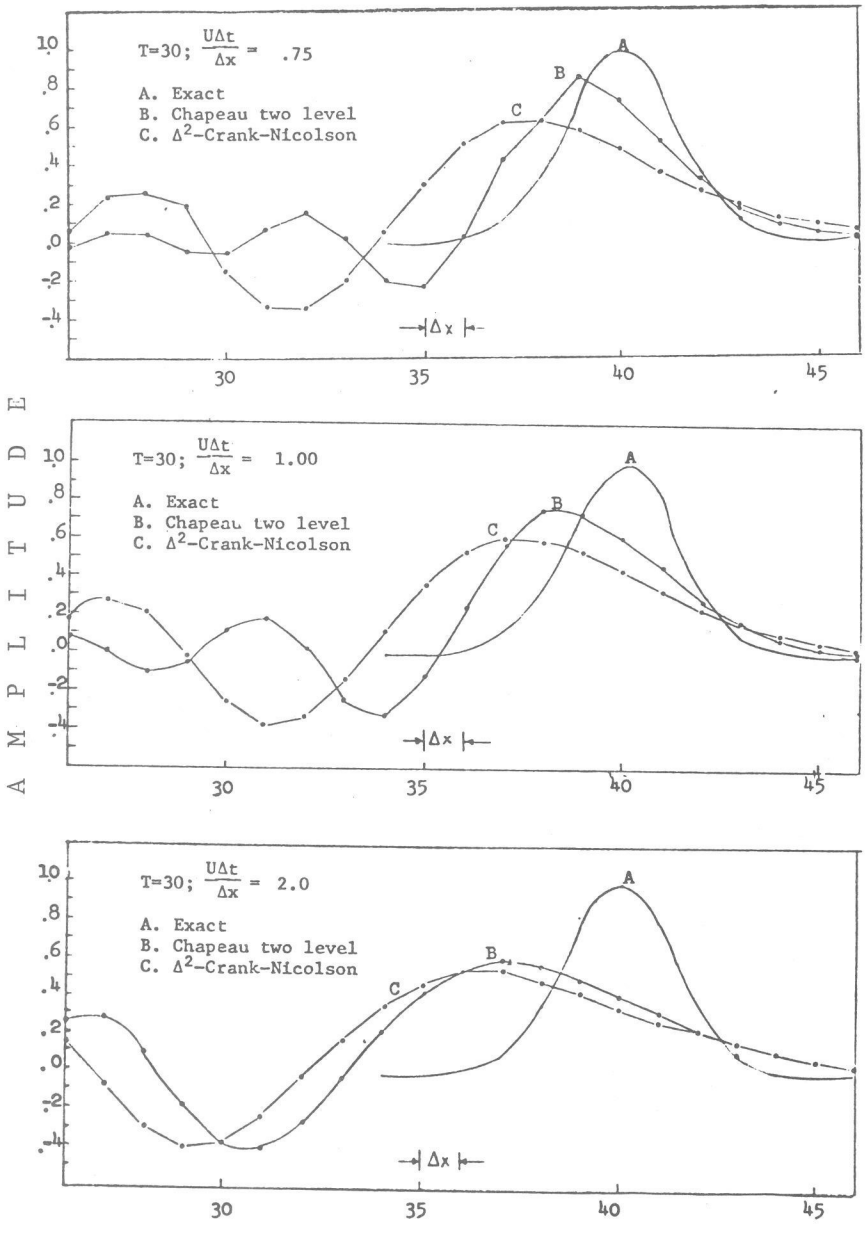

Figure 11.--Continued.

$$\frac{Q^{n+1} - Q^n}{\Delta t} + \frac{U}{2}\left[\frac{Q_{j+1}^{n+1} - Q_{j-1}^{n+1}}{2\Delta x} + \frac{Q_{j+1}^{n} - Q_{j-1}^{n}}{2\Delta x}\right] = 0.$$

Both the chapeau two-level and the Crank-Nicolson schemes permit unlimited time steps without instability. The Crank-Nicolson and second-order leap-frog schemes give nearly identical results for small Courant numbers. It is apparent that the chapeau function solution is much more accurate than the second-order scheme, with very little peak shift and only a slight wake. By comparison, the second-order scheme substantially diminishes the amplitude, creates a peak shift as large as the half-width, and produces a substantial wake. Neither scheme is dissipative; all errors result from dispersion.

As the time step is increased, the chapeau solution deteriorates, a phenomenon easily predicted from the fact that the spatial truncation error in Δx is of higher order than the temporal error in Δt.

Figure 11 shows that the distinction between the second- and fourth-order solution is fairly well retained up to a Courant number of 2 at which point the temporal truncation error swamps the spatial error. Small features are poorly handled at such large Courant numbers.

The deterioration also occurs for the non-linear equation when the Courant number is increased (figure 12). The results can be improved slightly by expressing the advective velocities approximately at time level $(n + 1/2)\ \Delta t$ by using

$$\beta^{n+1/2} = \beta^n - \beta^n \frac{\Delta t}{4\Delta x}(\beta_{j+1}^n - \beta_{j-1}^n).$$

Absolute instability would result if this relation were used separately as a finite-difference scheme, but confining its use to the advective terms improves results over the use of B^n alone.

The absence of the large wake, even for large peak Courant numbers in this and all of the other non-linear examples, evidently springs from the fact that the local Courant number at the rear of the Gaussian is small.

Both linear versions of the three-level chapeau function scheme (7.7-7.8) are slightly more accurate than the two-level version, but both are limited in the time step permitted. By expressing the spatial portion, B^n, of (7.7) as a weighted average of three time levels (7.5), the stability and accuracy of the three-level scheme may be improved (figure 13). As with the two-level scheme, there is the problem of supplying the advective velocity at $t=(n+1)\ \Delta t$ in the non-linear version; however, we found that linearizing the advective terms at each time step gave reasonably good results.

Turning now to the cubic spline solution of the linear equation (figure 14), we see that the spline solution does very well up to a Courant number of 0.3-0.4 with little peak shift and wake. The Courant number of 0.3 seems to be a transition point above which the diminution of the wake is accompanied by the advent of a forerunner and a positive peak shift. Both become particularly evident for $U\Delta t/\Delta x = 0.5$. We thought this behavior of initial

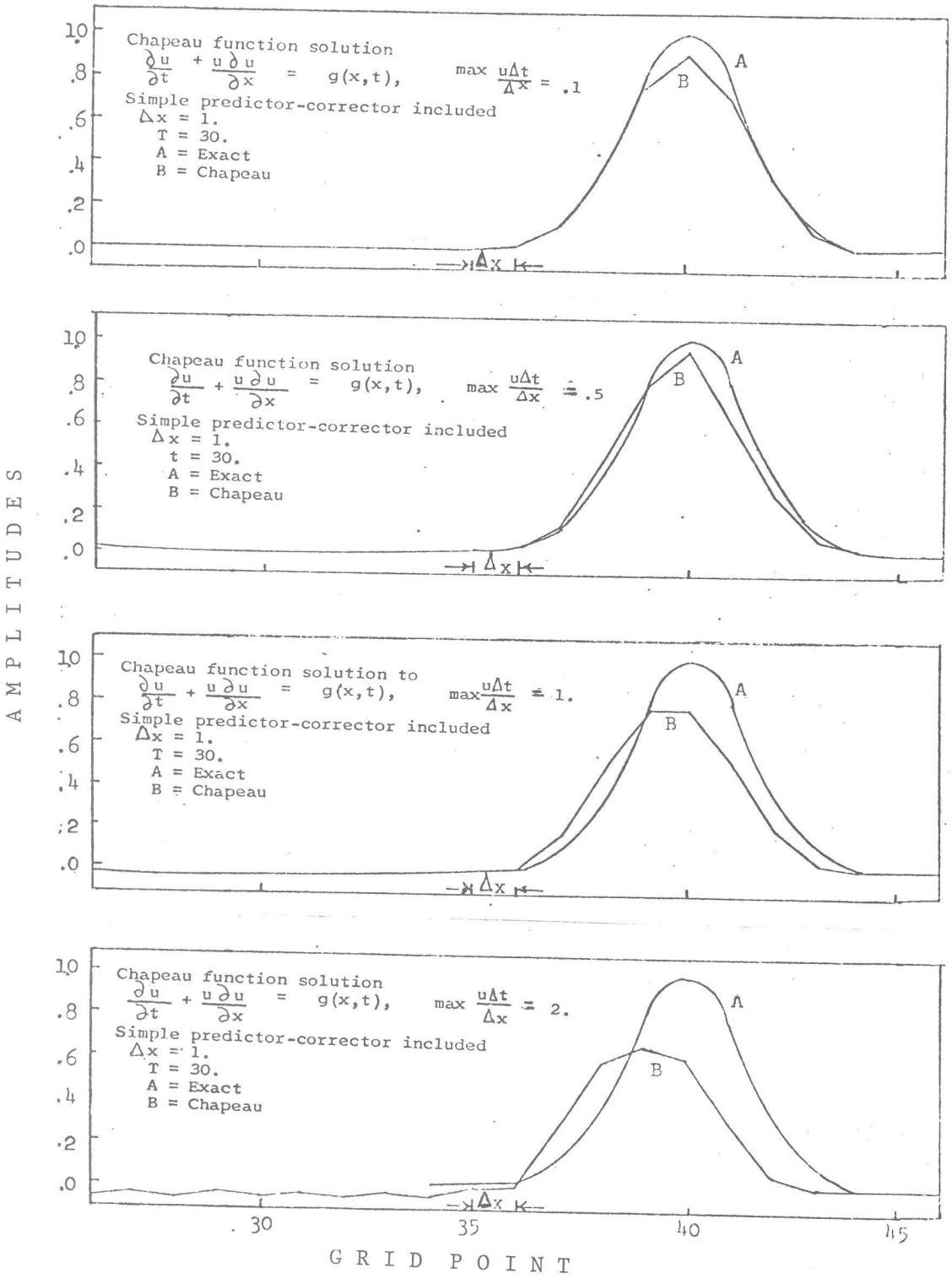

Figure 12.--Exact (curve A) and three-level chapeau function (curve B) solutions to the non-linear advection equation described in text.

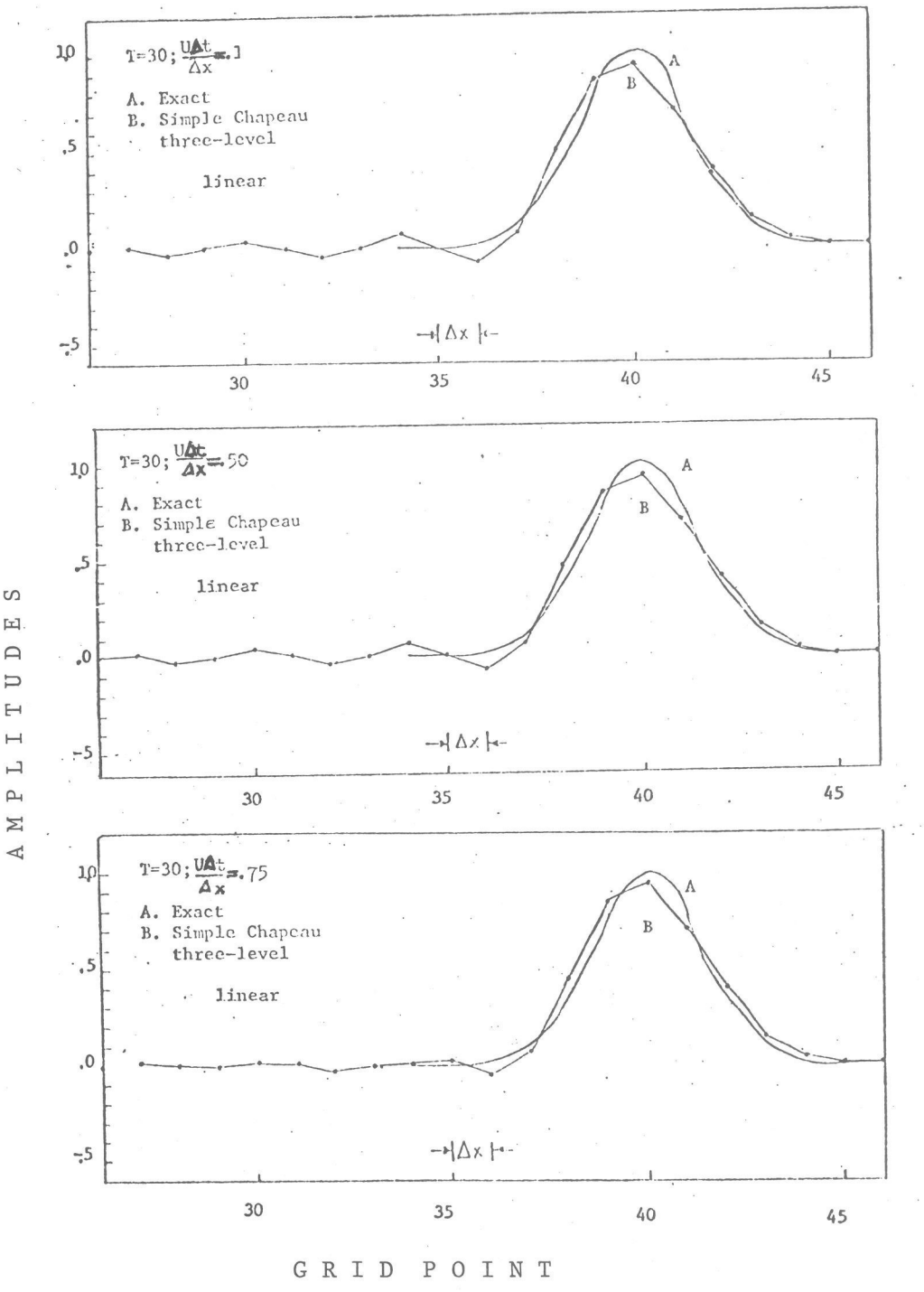

Figure 13.-- Exact (curve A) and three-level chapeau function (curve B) solutions to the linear advection equation.

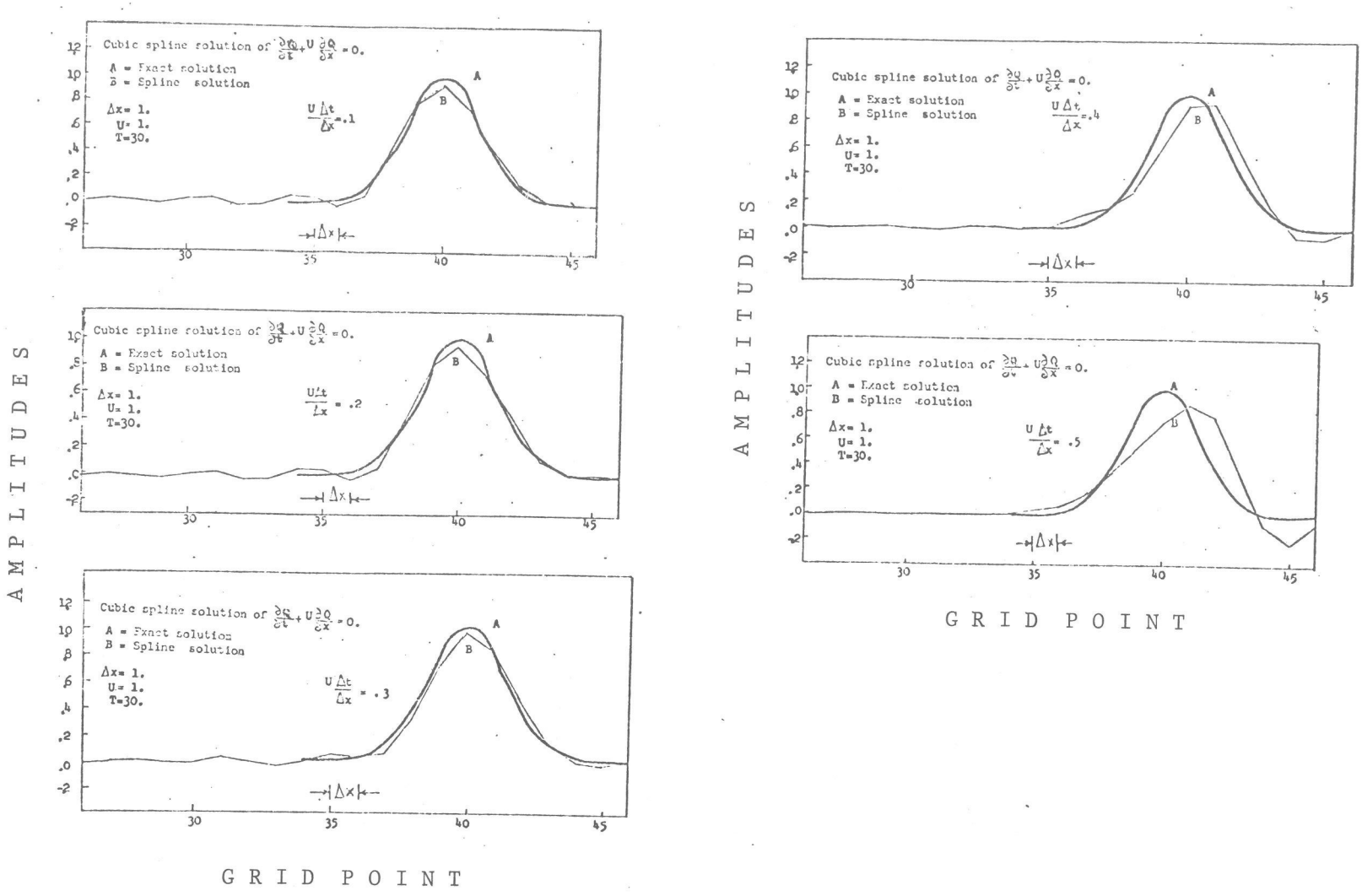

Figure 14.--Similar to figure 13, but cubic spline replaces chapeau function solution.

improvement and then degradation strange; the leap-frog and the chapeau three-level solutions improve as the Courant number approaches the schemes' stability limit, while the Crank-Nicolson and two-step chapeau function solutions degrade. At first we believed the creation of the forerunners marked the onset of a mild instability, but no amplification was noted when the running time was increased. Only when the Courant number was allowed to rise to 0.55-0.60 did observable instability occur.

This result was puzzling in light of the solution to the non-linear equation (figure 15). In the non-linear case, the solution improves as the Courant number increases to 0.4. A Courant number of 0.5 is enough to induce instability for the non-linear equation, even though the linear case retains its stability. Apparently examining the linear equation for clues to local stability of the non-linear case is not very useful in this instance.

Figure 16 is a remarkable illustration of the potential of an active telescoping grid. The outer region is coarser than the inner region by a factor of four. The Gaussian rapidly deteriorates as it moves through the coarse region until it enters the fine mesh portion where it begins to regain its original shape. As it re-enters the coarse region, the solution is very nearly exact (T=20). Passing again through the coarse mesh, the Gaussian deteriorates rapidly. The regeneration of the wave packet in this figure is an example of what can happen when the physics of a simulation is represented on a refined grid. In this case, the "physics" is the forcing term $g(x,t)$. The degradation would have been arrested but not reversed in the absence of the forcing term.

An unfortunate side effect of the telescoping grid is the reflection which occurs at the interface of fine-to-coarse mesh. It is probable the reflection can be mitigated by using a more gradual transition to the coarse mesh spacing.

X. SUMMARY AND CONCLUSIONS

The one-dimensional planetary boundary model described in this report simulates the diurnal variation in the wind, temperature, and humidity within the atmospheric boundary layer. The numerical solution is carried out by using a very long step (up to one half-hour) with a negligible deterioration in the solution. This feature (along with the efficient handling of the soil heat flux by means of an analytical solution rather than a system of computational levels) makes the extension of the one-dimensional model into a three-dimensional model economically feasible.

The Businger-Webb profile laws for the surface layer and the elementary O'Brien cubic K for the transition layer yield accurate predictions for surface temperature and fairly good predictions for surface wind. Partially because of the exclusion of advective effects, agreement between predicted and measured transition layer values is less successful than at the surface. In addition, there appear to be at least two other reasons for error: (a) Individual measurements show distinctly non-diurnal effects, and (b) The published values of the geostrophic wind have large experimental errors.

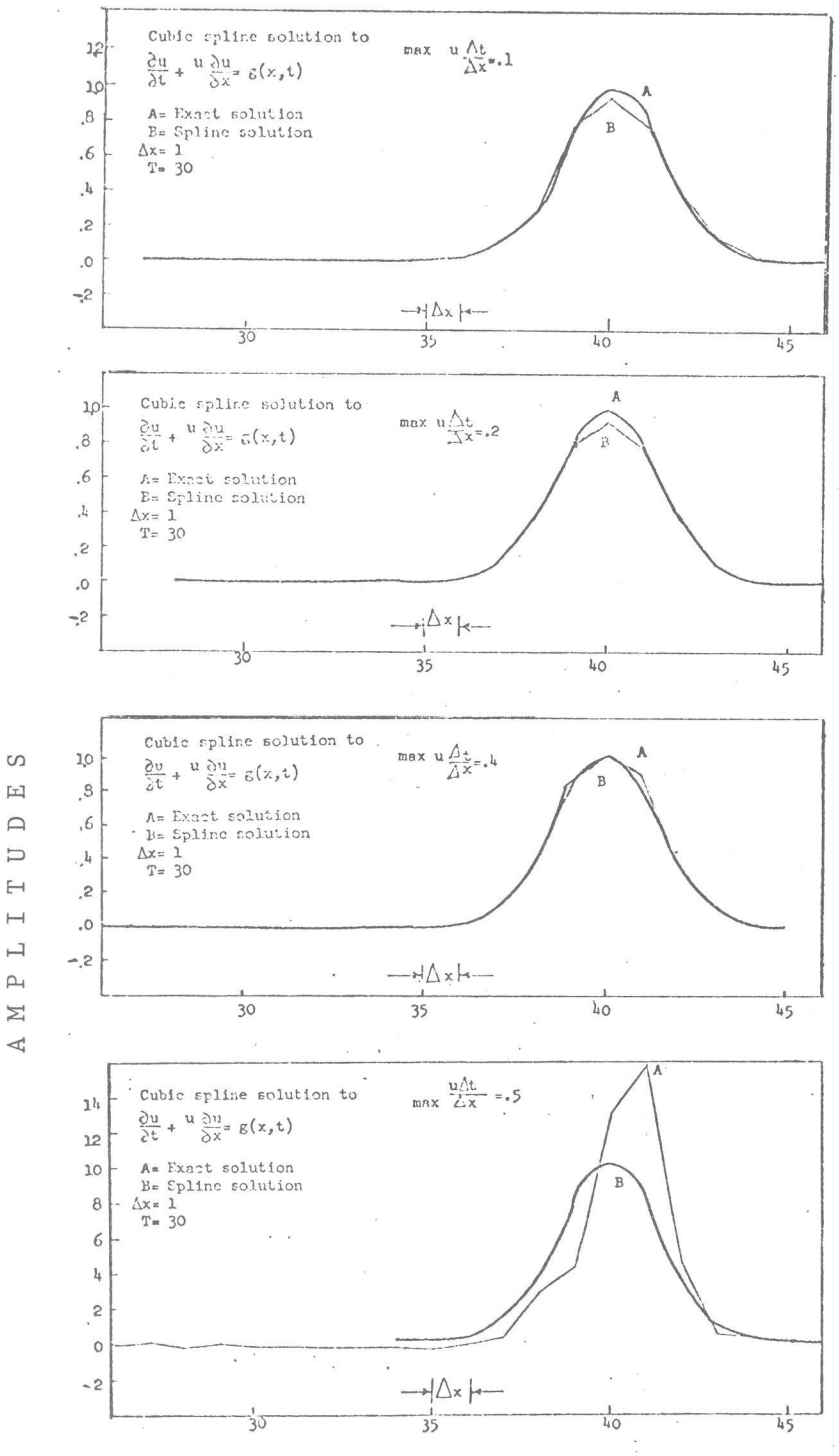

Figure 15.-- Same as figure 14, but non-linear advection equation replaces linear advection equation.

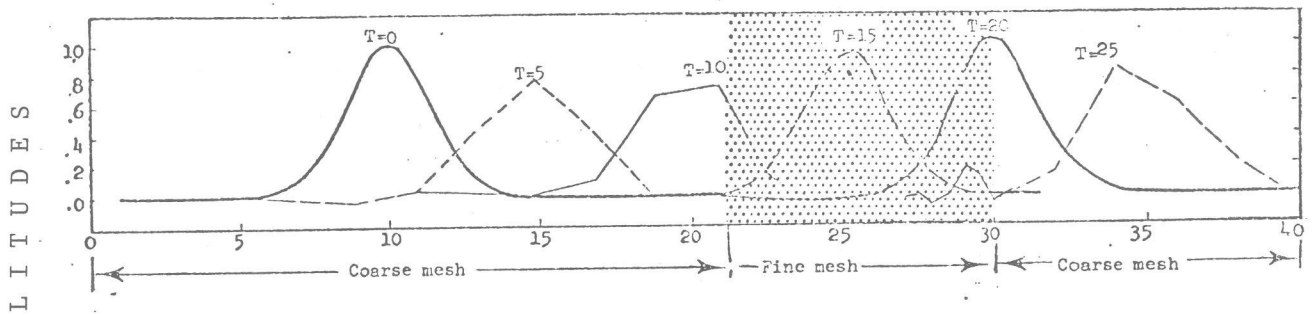

Evolution of Gaussian solution of $\frac{\partial u}{\partial t} + u\frac{\partial u}{\partial x} = g(x,t)$ as Gaussian passes from coarse mesh into fine mesh and back into coarse mesh.

max u= 1.

$\Delta t = .1$

$(\Delta x)_{coarse} = 2.$; $(\Delta x)_{fine} = .5$

Figure 16.-- Evolution of Gaussian solution of non-linear advection equation as Gaussian passes from coarse mesh into fine mesh (shaded region) and back into coarse mesh.

Computations show that neglecting the local radiative cooling can lead to unreasonably large nocturnal inversions. Radiative effects apparently extend to several hundred meters and serve to mitigate such extreme inversions.

The use of cubic splines and chapeau functions in the advection equation can greatly reduce dispersion errors characteristic of second-order finite-difference schemes. Cubic splines are used in a manner similar to the derivative of a Fourier series in the pseudo-spectral approximation; one merely replaces the second-order spatial derivatives with derivatives computed by cubic splines. The technique yields higly accurate derivatives; while the method seems less accurate than the pseudo-spectral solution to the advection equation, the spline technique has the advantage of being directly applicable to grids with unequal node spacing. An example is given in which a telescoping grid (a fine mesh surrounded by a coarse mesh) restores and preserves the wave packet which passes through it. However, spline interpolation is not free of all the problems of telecoping grids. The example clearly shows a reflection of a portion of the waves when a feature passes from the fine mesh region back into the coarse mesh region.

The chapeau function technique approximates the state of a feature by means of hat-like basis functions. A differential-difference equation for the coefficients results from the substitution of the chapeau solution into the advection equation. The stability and accuracy of the final solution depend upon the solution of the differential equation; a Crank-Nicolson approach leads to an abolutely stable solution with gradually deteriorating fidelity as the time step is increased. Other suggested approaches are more accurate but have stability criteria which must be satisfied. As with the spline technique, chapeau functions can be easily applied to grids of unequally spaced nodes. The chapeau function method can be applied to more than one spatial dimension by the technique of splitting.

Acknowledgment

The authors wish to thank Miss Farnese Hicks for her assistance in programming and analysis, Mr. Denis Sakelaris for preparing the figures, and both Mrs. Jocelyn Boss and Mrs. Sandra Swab for typing the text.

REFERENCES

Ahberg, J. H., E. N. Nilson, and J. L. Walsh, 1967: The Theory of Splines and their Applications. Academic Press, New York, 284 pp.

Businger, J. A., J. C. Wyngaard, Y. Izumi, and E. F. Bradley, 1971: Flux-profile relationships in the atmospheric surface layer. J. Atmos. Sci., 28, 181-189.

Clarke, R. H., A. J. Dyer, R. R. Brook, D. G. Reid, and A. J. Troup, 1971: The Wangara experiment: Boundary layer data. Commonwealth Scientific and Industrial Research Organization, Victoria, Australia, 349 pp.

Dyer, A. J., 1967: The turbulent transport of heat and water vapor in an unstable atmosphere. Quart. J. R. Met. Soc., 93, 501-508.

Krishna, K., 1968: A numerical study of the diurnal variations of meteorological parameters in the planetary boundary layer: I. Diurnal variation of winds. Monthly Weather Review, 96, 269-276.

Lettau, H. H., and B. Davidson, 1957: Exploring the atmosphere's first mile. Pergamon Press, New York, 578 pp.

Long, P. E., 1973: Dissipation, dispersion and difference schemes. Presented at WMO/IAMAP Conference on Mesoscale Representation and Fine Mesh Modeling, May 14-18, 1973, Shinfield Park, Reading, Berkshire, U.K.

O'Brien, J. J., 1970: A note on the vertical structure of the eddy exchange coefficient in the planetary boundary layer. J. Atmos. Sci., 27, 1213-1215.

Obukhov, A. M., 1946: Turbulence in an atmosphere with a non-uniform temperature. Trudy Instituta Teoreticheskio Geofiziki ANSSR. Translated and reprinted in Boundary-Layer Meteorology, 1971, 2, 3-29.

Price, G. V., and A. K. MacPherson, 1973: A numerical weather forecasting method using cubic splines on a variable mesh. J. Appl. Meteor., 12, 1102-1113.

Shaffer, W. A., and P. E. Long, 1973: A predictive boundary layer model. Presented at the Symposium on the Atmospheric Boundary Layer, Oct. 10-12, 1973, Mainz, Germany.

Webb, E. K., 1970: Profile relationships: The log-linear range, and extension to strong stability. Quart. J. R. Met. Soc., 96, 67-90.

Yanenko, N. A., 1971: The Method of Fractional Steps. Springer-Verlag, Heidelberg, 160 pp.

(Continued from inside front cover)

WBTM TDL 25 Charts Giving Station Precipitation in the Plateau States From 850- and 500-Millibar Lows During Winter. August F. Korte, Donald L. Jorgensen, and William H. Klein, September 1969. (PB-187-476)

WBTM TDL 26 Computer Forecasts of Maximum and Minimum Surface Temperatures. William H. Klein, Frank Lewis, and George P. Casely, October 1969. (PB-189-105)

WBTM TDL 27 An Operational Method for Objectively Forecasting Probability of Precipitation. Harry R. Glahn and Dale A. Lowry, October 1969. (PB-188-660)

WBTM TDL 28 Techniques for Forecasting Low Water Occurrences at Baltimore and Norfolk. James M. McClelland, March 1970. (PB-191-744)

WBTM TDL 29 A Method for Predicting Surface Winds. Harry R. Glahn, March 1970. (PB-191-745)

WBTM TDL 30 Summary of Selected Reference Material on the Oceanographic Phenomena of Tides, Storm Surges, Waves, and Breakers. N. Arthur Pore, May 1970. (PB-192-449)

WBTM TDL 31 Persistence of Precipitation at 108 Cities in the Conterminous United States. Donald L. Jorgensen and William H. Klein, May 1970. (PB-193-599)

WBTM TDL 32 Computer-Produced Worded Forecasts. Harry R. Glahn, June 1970. (PB-194-262)

WBTM TDL 33 Calculation of Precipitable Water. L. P. Harrison, June 1970. (PB-193-600)

WBTM TDL 34 An Objective Method for Forecasting Winds Over Lake Erie and Lake Ontario. Celso S. Barrientos, August 1970. (PB-194-586)

WBTM TDL 35 Probabilistic Prediction in Meteorology: a Bibliography. Allan H. Murphy and Roger A. Allen, June 1970. (PB-194-415)

WBTM TDL 36 Current High Altitude Observations--Investigation and Possible Improvement. M. A. Alaka and R. C. Elvander, July 1970. (COM-71-00003)

NOAA Technical Memoranda

NWS TDL-37 Prediction of Surface Dew Point Temperatures. R. C. Elvander, February 1971. (COM-71-00253)

NWS TDL-38 Objectively Computed Surface Diagnostic Fields. Robert J. Bermowitz, February 1971. (COM-71-00301)

NWS TDS-39 Computer Prediction of Precipitation Probability for 108 Cities in the United States. William H. Klein, February 1971. (COM-71-00249)

NWS TDL-40 Wave Climatology for the Great Lakes. N. A. Pore, J. M. McClelland, C. S. Barrientos, and W. E. Kennedy, February 1971. (COM-71-00368)

NWS TDL-41 Twice-Daily Mean Monthly Heights in the Troposphere Over North America and Vicinity. August F. Korte, June 1971. (COM-71-00826)

NWS TDL-42 Some Experiments With a Fine-Mesh 500-Millibar Barotropic Model. Robert J. Bermowitz, August 1971. (COM-71-00958)

NWS TDL-43 Air-Sea Energy Exchange in Lagrangian Temperature and Dew Point Forecasts. Ronald M. Reap, October 1971. (COM-71-01112)

NWS TDL-44 Use of Surface Observations in Boundary-Layer Analysis. H. Michael Mogil and William D. Bonner, March 1972. (COM-72-10641)

NWS TDL-45 The Use of Model Output Statistics (MOS) To Estimate Daily Maximum Temperatures. John R. Annett, Harry R. Glahn, and Dale A. Lowry, March 1972. (COM-72-10753)

NWS TDL-46 SPLASH (Special Program To List Amplitudes of Surges From Hurricanes) I. Landfall Storms. Chester P. Jelesnianski, April 1972. (COM-72-10807)

NWS TDL-47 Mean Diurnal and Monthly Height Changes in the Troposphere Over North America and Vicinity. August F. Korte and DeVer Colson, August 1972. (COM-72-11132)

NWS TDL-48 Synoptic Climatological Studies of Precipitation in the Plateau States From 850-, 700-, and 500-Millibar Lows During Spring. August F. Korte, Donald L. Jorgensen, and William H. Klein, August 1972. (COM-73-10069)

NWS TDL-49 Synoptic Climatological Studies of Precipitation in the Plateau States From 850-Millibar Lows During Fall. August F. Korte and DeVer Colson, August 1972. (COM-74-10464)

NWS TDL-50 Forecasting Extratropical Storm Surges For the Northeast Coast of the United States. N. Arthur Pore, William S. Richardson, and Herman P. Perrotti, January 1974. (COM-74-10719)

NWS TDL-51 Predicting the Conditional Probability of Frozen Precipitation. Harry R. Glahn and Joseph R. Bocchieri, March 1974. (COM-74-10909/AS)

NWS TDL-52 SPLASH (Special Program to List Amplitudes of Surges From Hurricanes) II. General Track and Variant Storm Conditions. Chester P. Jelesnianski, March 1974.

NWS TDL-53 A Comparison Between the Single Station and Generalized Operator Techniques for Automated Prediction of Precipitation Probability. Joseph R. Bocchieri, September 1974. (COM-74-11763/AS)

NWS TDL-54 Climatology of Lake Erie Storm Surges at Buffalo and Toledo. N. Arthur Pore, Herman P. Perrotti, and William S. Richardson, December 1974.

NWS TDL-55 Dissipation, Dispersion and Difference Schemes. Paul E. Long, Jr, in press, 1975.